

Tectonics

RESEARCH ARTICLE

10.1029/2019TC005874

This article is a companion to Abdulhameed et al. (2020) <https://doi.org/10.1029/2019TC005873>, Gagala et al. (2020) <https://doi.org/10.1029/2019TC005871>.

Key Points:

- Onset of synorogenic sedimentation in the Khingou Formation ($\leq \sim 23\text{--}12$ Ma) indicates orogenic front progression from Central to North Pamir
- Growth strata in the Tavildara Formation ($\leq \sim 15\text{--}5$ Ma) record Tajik fold-thrust belt formation triggered by India-Asia lithosphere collision
- Cessation of growth strata formation and proximal floodplain deposition between ~ 5 and 4 Ma reflects Tajik lithosphere rollback

Supporting Information:

- Supporting Information S1
- Data S1
- Data S2

Correspondence to:

R. Dedow, and L. Ratschbacher, ralf@dedow.de; lothar@geo.tu-freiberg.de

Citation:

Dedow, R., Franz, M., Szulc, A., Schneider, J. W., Brückner, J., Ratschbacher, L., et al. (2020). Tajik Basin and Southwestern Tian Shan, Northwestern India-Asia collision zone: 3. Preorogenic to synorogenic retro-foreland basin evolution in the eastern Tajik depression and linkage to the Pamir hinterland. *Tectonics*, 39, e2019TC005874. <https://doi.org/10.1029/2019TC005874>

Received 3 SEP 2019

Accepted 8 FEB 2020






Accepted article online 19 MAR 2020

[Correction added on 27 JULY 2020, after first online publication: Projekt Deal funding statement has been added.]

©2020. The Authors.

This is an open access article under the terms of the Creative Commons Attribution License, which permits use, distribution and reproduction in any medium, provided the original work is properly cited.

Tajik Basin and Southwestern Tian Shan, Northwestern India-Asia Collision Zone: 3. Preorogenic to Synorogenic Retro-foreland Basin Evolution in the Eastern Tajik Depression and Linkage to the Pamir Hinterland

Ralf Dedow¹ , Matthias Franz^{1,2} , Adam Szulc^{1,3} , Jörg W. Schneider^{1,4}, Jan Brückner¹, Lothar Ratschbacher¹ , Łukasz Gagala¹, Jean-Claude Ringenbach⁵, Negmat Rajabov⁶, Mustaf Gadoev⁶ , and Ilhomjon Oimahmadov⁶

¹Geologie, TU Bergakademie Freiberg, Freiberg, Germany, ²Now at Geoscience Center, University of Göttingen, Göttingen, Germany, ³Now at CASP, Cambridge, UK, ⁴Geology and Petroleum Technologies, Kazan Federal University, Kazan, Russia, ⁵E2S-UPPA, CNRS, University Pau and Pays Adour, Pau, France, ⁶Institute of Geology, Earthquake Engineering and Seismology, Tajik Academy of Sciences, Dushanbe, Tajikistan

Abstract The Tajik basin archives the orogenic evolution of the Pamir hinterland. Stratigraphic-sedimentologic observations from Cretaceous-Pliocene strata along its eastern margin describe the depositional environment and basin-formation stages in reaction to hinterland exhumation and basin inversion. During the Late Cretaceous-Eocene (preorogenic stage: $\sim 100\text{--}34$ Ma), a shallow-marine to terrestrial basin extended throughout Central Asia. An alluvial plain with influx of conglomerate bodies (Baljuvon Formation) indicates a first pulse of hinterland erosion and foreland-basin formation in the late Oligocene-early Miocene (synorogenic stage Ia: $\sim 34\text{--}23$ Ma). Further hinterland exhumation deposited massive alluvial conglomerates (Khingou Formation) in the early-middle Miocene (synorogenic stage Ib: $\sim 23\text{--}15$ Ma). Westward thickening growth strata suggest transformation of the Tajik basin into the Tajik fold-thrust belt in the middle-late Miocene (synorogenic stage IIa: $\sim 15\text{--}5$ Ma). Increased water supply led to the formation of fluvial mega-fans (Tavildara Formation). Latest Miocene-Pliocene shortening constructed basin morphology that blocked sediment bypass into the central basin from the east (Karanak Formation), triggering drainage-system reorganization from transverse to longitudinal sediment transport (synorogenic stage IIb: $< \sim 5$ Ma). Accelerated shortening ($\sim 27\text{--}20$ Ma) and foreland-directed collapse ($\sim 23\text{--}12$ Ma) of Pamir-plateau crust loaded the foreland and induced synorogenic stages Ia and Ib. Coupling of Indian and Asian cratonic lithospheres and onset of northward and westward delamination/rollback of Asian lithosphere (i.e., lithosphere of the Tajik basin) beneath the Pamir at $\sim 12\text{--}11$ Ma transformed the Tajik basin into the Tajik fold-thrust belt (synorogenic stage IIa). The timing of the sedimentologically derived basin reconfiguration matches the thermochronologically derived onset of Tajik-basin inversion at ~ 12 Ma.

1. Introduction: Retro-foreland Tajik Basin and Possible Foreland-Hinterland Coupling

Sedimentologic processes along the margins of continental foreland basins record the progradation of shortening and exhumation in the orogenic hinterland (e.g., DeCelles & Giles, 1996). Accordingly, the foreland basins fringing the Pamir-Tibet orogen have served as archives for tracing the India-Asia collision from its onset at ~ 50 Ma to Present (e.g., Allen et al., 1991; Bande et al., 2015; DeCelles et al., 1998; Einsele, 1996; Najman et al., 2009; Wang et al., 2013; Xiao et al., 2012; Zheng et al., 2006). One underexplored archive is the Tajik basin in the Afghan-Tajik depression west of the Pamir salient (Figures 1a to 1c). Its up to 10-km-thick deposits comprise Triassic-Oligocene preorogenic strata of alternating shallow-marine to continental facies, and Miocene-Pliocene synorogenic clastic continental deposits, sourced from the rising Pamir in the east, the Hindu Kush in the south, and the Tian Shan in the north (e.g., Burtman & Molnar, 1993; Carrapa et al., 2015; Chapman et al., 2019; Dzhililov et al., 1982; Klocke et al., 2017). Most research on the synorogenic deposits dates back to the 1960s–1980s (e.g., Bosov, 1961, 1972; Dzhililov et al., 1982; Leonov, 1977; Schwab et al., 1980). Modern facies analysis, in particular on the synorogenic foreland-basin strata, will—together with studies in the hinterland—enable an understanding of the coupling between the evolution of this retro-foreland basin and its orogenic hinterland—the Pamir.

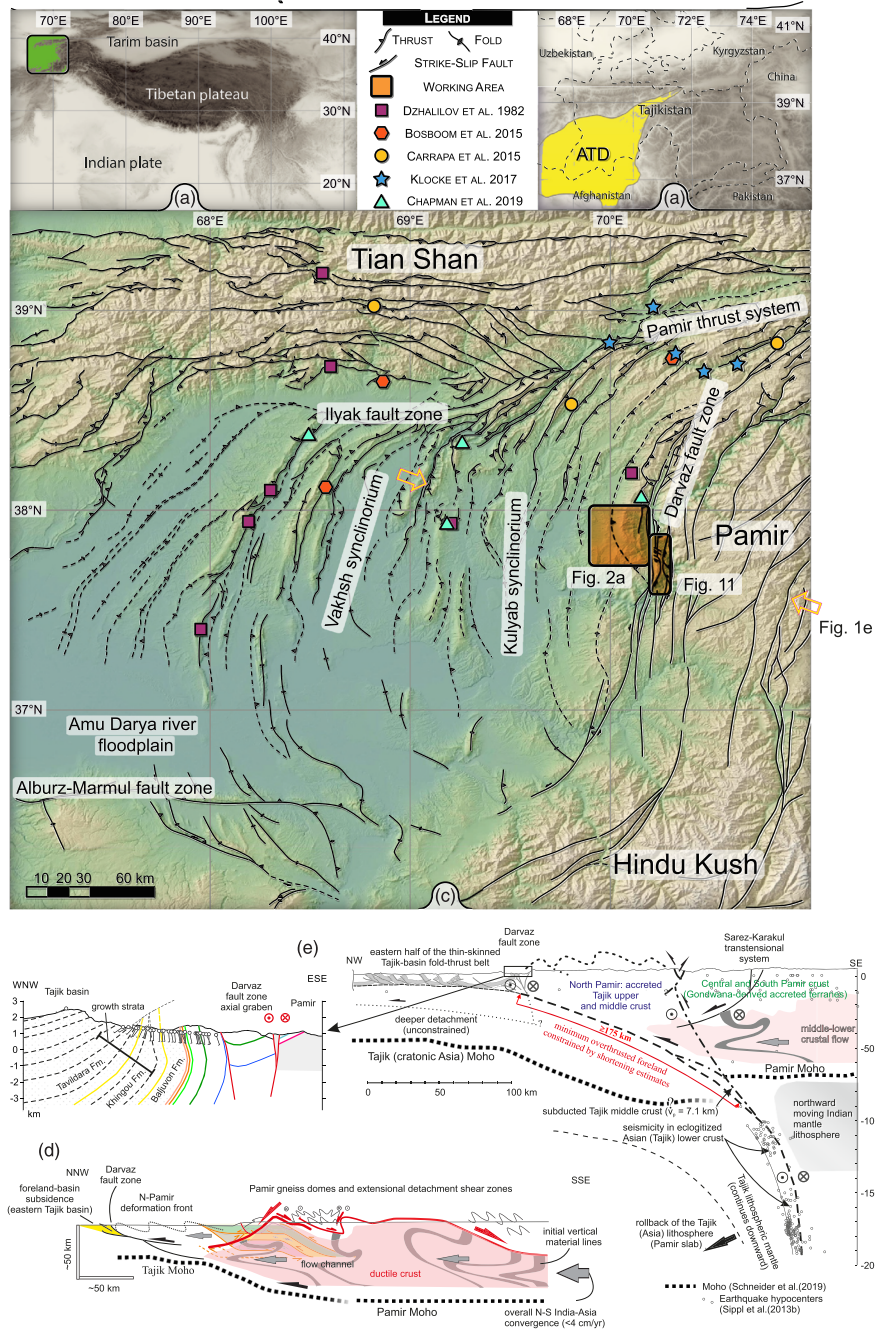


Figure 1. (a) The Afghan-Tajik depression (green frame) in the India-Asia collision zone. (b) The Afghan-Tajik depression in the geography of Central Asia. (c) Digital elevation model of the Afghan-Tajik depression and its surrounding mountain belts with the major fault and fold traces modified from Abdulhameed et al. (2020). The Tajik basin is the part of the Afghan-Tajik depression north of the Amu-Darya floodplain and west of the Darvaz fault zone. The orange rectangles locate the study areas at the eastern margin of the Tajik basin. (d) Cross-sectional sketch of the ~23- to 15-Ma evolution of the Pamir and is foreland modified from Abdulhameed et al. (2020). The ~37- to 20-Ma crustal thickening is sketched by the thrust stacks and recumbent fold nappes of the Central Pamir. The ~23- to 15-Ma collapse of the Pamir-plateau crust transferred the deformation front from the Central to the North Pamir inducing foreland subsidence. The ductile crust (red) is dragging the middle and upper crust foreland-ward. The model geometries and kinematics are akin to models proposed for foreland-directed plateau collapse (e.g., Rey et al., 2010). (e) Cross-sectional sketch of the constraints imposed by the foreland shortening of the Tajik crust on the geometry of the Tajik lithosphere beneath the Pamir (modified from Gagala et al., 2020, and Abdulhameed et al., 2020). The seismicity cluster and subducted Tajik middle crust approximate the down-dip extension of the detachments of the Tajik foreland. This geometry defines the curved upper interface of the rolling back Tajik lithosphere. The shortening estimates in the western Tian Shan and the Tajik fold-thrust belt and the yet unquantified amounts of accretion and deep subduction of Tajik upper and middle crust in and beneath the North Pamir are considered a proxy for the amount of convergence since ~12 Ma. The sinistral-normal Karakul-Sarez fault system and the red zone on the right side of the cross section highlight the upper to lower crustal flow of the Pamir-plateau crust toward the foreland. See text for references and discussion.

The Afghan-Tajik depression covers $\sim 44,000$ km² and stretches from western Tajikistan and southeastern Uzbekistan to northern Afghanistan (Figure 1b). Its boundaries in the north, east, and south are, respectively, the broad dextral transpressive deformation zone in the southwestern Tian Shan (Babaev, 1988; Käßner et al., 2016), the sinistral Darvaz fault zone (e.g., Trifonov, 1978), and the dextral-reverse Alburz-Marmul fault zone (e.g., Wellman, 1966). The Amu Darya river drains the depression to the Aral Sea. The inversion of the depression into the Tajik fold-thrust belt since the Miocene (e.g., Abdulhameed et al., 2020; Chapman et al., 2017, 2019; Gaęala et al., 2020; Hamburger et al., 1992; Kufner et al., 2018; Leith & Alvarez, 1985; Nikolaev, 2002) has produced arcuate, grossly N trending synform and antiforms, subparallel to the western edge of the Pamir; the antiforms are defined by intrabasin mountain ranges (Figure 1c). About E-W shortening in the fold-thrust belt was accompanied by anticlockwise rotation (e.g., Pozzi & Feinberg, 1991; Thomas et al., 1994) that decreases from up to 50° to negligible from the Pamir margin to the western foreland buttress. Excellent outcrop of the Mesozoic-Cenozoic strata along the depression's eastern margin (Figure 1c) allows the reconstruction of the basin evolution, in particular the coupling between the hinterland tectonics and foreland response. In the following, we refer to the Tajik part of the Afghan-Tajik depression—our working area—as the Tajik basin.

Geologic, geophysical, structural, and geo-thermochronologic studies in the Pamir outline a prolonged but phased shortening history, accompanied by synorogenic, upper to locally lower crustal extension. These events—with the bulk displacement directions parallel to the India-Asia convergence—are accompanied by lateral extrusion, that is, out-of-the-orogen, mostly west directed material flow (e.g., Kufner et al., 2018; Rutte, Ratschbacher, Schneider, et al., 2017; Rutte, Ratschbacher, Khan, et al., 2017; Schurr et al., 2014; Worthington et al., 2020). This evolution appears to be driven by lithosphere-scale processes that caused first-order changes in the orogen at ~ 23 –19 Ma and ~ 12 –11 Ma. Thickening of the Asian (“Gondwana”) crust in the Central and South Pamir has been active since at least 37 Ma, accelerated after ~ 27 Ma, and switched to crustal extension at ~ 23 –19 Ma (Hacker et al., 2017; Rutte, Ratschbacher, Schneider, et al., 2017; Rutte, Ratschbacher, Khan, et al., 2017; Stübner, Ratschbacher, Rutte, et al., 2013; Stübner, Ratschbacher, Weise, et al., 2013; Stearns et al., 2013, 2015; Smit et al., 2014; Worthington et al., 2020). The change from crustal shortening to extension at ~ 23 –19 Ma was contemporaneous with the proposed slab breakoff of Greater India from cratonic India, which likely triggered gravitational collapse of the Pamir-plateau crust (e.g., DeCelles et al., 2011; Replumaz et al., 2010; Rutte, Ratschbacher, Schneider, et al., 2017; Rutte, Ratschbacher, Khan, et al., 2017; Stearns et al., 2013, 2015). Accelerated thickening, overall foreland advance of the orogen due to the India-Asia convergence, and in particular the crustal collapse explain the relocation of the deformation front from the Central Pamir to the North Pamir at this time (Rutte, Ratschbacher, Schneider, et al., 2017; Rutte, Ratschbacher, Khan, et al., 2017).

Kufner et al. (2016) inferred that northward advancing cratonic Indian lithosphere underneath the Pamir is currently forcing rollback of Asian (“Tajik”) lithosphere—the basement of the Tajik-Tarim basins, including that of the North Pamir. In the Pamir, the southern edge of this Tajik lithosphere must have been positioned ~ 380 km south of its present-day position and was roughly aligned with the southern, present-day margins of the Tajik and Tarim basins west and east of the Pamir. They calculated that delamination/rollback of ~ 380 km of this lithosphere has taken ~ 12 –11 Myr. The northward and westward rollback since ~ 12 Ma may explain the neotectonic deformation along the Pamir front and its western foreland. Dominant $\sim N$ -S shortening is accompanied by westward flow (lateral extrusion) of Pamir-plateau crust into the Afghan-Tajik depression where it is causing thin-skinned shortening of the Tajik-basin sediments above a décollement in Jurassic evaporites, producing the Tajik fold-thrust belt (Figure 1c; e.g., Gaęala et al., 2020; Kufner et al., 2018; Nikolaev, 2002; Rutte, Ratschbacher, Schneider, et al., 2017; Rutte, Ratschbacher, Khan, et al., 2017; Stübner, Ratschbacher, Rutte, et al., 2013; Schurr et al., 2014). Using thermochronology, Abdulhameed et al. (2020) showed that inversion of the Tajik basin indeed started at ~ 12 Ma.

In Figures 1d and 1e, we visualize diagrammatically the first-order geometries and kinematics of the ~ 23 - to 15-Ma and ~ 12 - to 0-Ma tectonic events in hinterland (Pamir plateau) to foreland (North Pamir and Tajik basin) cross sections. In Figure 1d, adopted from Abdulhameed et al. (2020), the ~ 37 - to 19-Ma crustal thickening is schematically shown by the thrust stacks and recumbent fold nappes of the Central Pamir (Hacker et al., 2017; Rutte, Ratschbacher, Schneider, et al., 2017; Rutte, Ratschbacher, Khan, et al., 2017). Thickening was followed by gravitational collapse of the upper to (locally lower) crust of the Pamir plateau along the

normal-sense shear zones of the Central Pamir and South Pamir during the formation of the Pamir gneiss domes (extensional metamorphic core complexes). The ~23- to 19-Ma onset of collapse of the leading edge of the Pamir plateau in the Central Pamir is interpreted to propel shortening north and northwest of it, transferring the deformation from the Central to the North Pamir (Rutte, Ratschbacher, Schneider, et al., 2017; Rutte, Ratschbacher, Khan, et al., 2017; Stübner, Ratschbacher, Rutte, et al., 2013; Stübner, Ratschbacher, Weise, et al., 2013; Worthington et al., 2020). The ductile crust (red in Figure 1d) likely contains a crustal flow channel, dragging the middle and upper crust foreland-ward. The geometries and kinematics are akin to models of foreland-directed plateau collapse (e.g., Rey et al., 2010; their Figures 2 and 3).

Figure 1e sketches the constraints imposed by the ~12- to 0-Ma foreland shortening of the Tajik crust on the geometry of the Tajik lithosphere beneath the Pamir (modified from Gałała et al., 2020). The seismicity cluster in the Tajik lower crust and the subducted Tajik middle crust (Sippl, Schurr, Yuan, et al., 2013; Sippl, Schurr, Tympel, et al., 2013) approximate the down-dip extension of the detachments of the Tajik foreland. This geometry defines the curved upper interface of the rolling back Tajik-basin lithosphere; it is mirrored by the Tajik Moho, traced down to ~90 km (Schneider et al., 2019). The ≥ 175 -km shortening estimates in the Tian Shan foreland and the inverted Tajik basin—the Tajik fold-thrust belt (Gałała et al., 2020)—and the yet unquantified amounts of accretion and deep subduction (Sippl, Schurr, Tympel, et al., 2013) of Tajik upper-middle crust beneath the North Pamir are proxies for the amount of convergence since ~12 Ma. The sinistral-normal Karakul-Sarez fault system and the red zone on the right side of the cross section sketch the upper to lower crustal flow from the thick Pamir-plateau crust to the foreland depression (Stübner, Ratschbacher, Rutte, et al., 2013; Sass et al., 2014). The inset on the left in Figure 1e shows the structural-stratigraphic features at the current eastern erosional margin of the Tajik basin. The sinistral strike-slip geometry of the active Darvaz fault zone is at odds with the thin-skinned shortening of the Tajik fold-thrust belt that cannot be conveyed across a vertical fault interface. Likely, this geometry and kinematics is a young feature, largely postdating the thin-skinned thrusting in the Tajik fold-thrust belt (cf. Kufner et al., 2018).

Herein, we use stratigraphic and sedimentologic observations from Cretaceous-Pliocene strata along the eastern margin of the Tajik basin—the Shurobod area (Figure 2)—to describe the depositional environment, drainage-system evolution, and stages of basin formation in reaction to the progressive hinterland exhumation and inversion of the Tajik basin. These are combined with data from sediment petrography and geochemistry to detect source-area changes in the hinterland. In particular, we define distinct stages of the evolution of the Tajik basin, that is, the change from the epi-continental to the synorogenic foreland basin, and the evolution of the synorogenic foreland basin into a foreland fold-thrust belt. Furthermore, we aim to link the phased evolutions of both the Tajik basin and the Pamir hinterland. We suggest that the crustal thickening and ultimately the collapsing Pamir-plateau crust loaded the foreland, causing the initial phase and the major phase of subsidence at ~34–23 and ~23–15 Ma, respectively, when a foreland basin was established. The coupling between the Indian and Asian lithospheres initiated the Tajik-basin inversion, that is, the switch from the foreland basin to the fold-thrust belt and the major phase of Tian Shan mountain building at ~12 Ma.

2. Working Area and Methods

Our sedimentologic analysis integrates field-based sedimentology, lithofacies analysis, petrography, and inorganic geochemistry of an ~500-km² area in the Shurobod region of the eastern Tajik basin (Figures 1 and 2). There, the Lower Cretaceous-Neogene, preorogenic to synorogenic basin fill is exposed in ~N trending ranges, stretching from the Panj-River valley in the east to the city of Kulyab (Figure 2a) in the west. Continuous exposure is accessible in W and SW trending gorges and along the road from Shurobod to the Panj and Parapanj valleys (Figure 2a; sections Shurobod Pass, Chilishtak One, Chilishtak Two, Shurobod South, and Shurobod North) and along the northern Panj valley (section Obi Khudkham). We studied further exposures around Imam Askar (section Imam Askar), the highest range of the Shurobod area, along the road from Shurobod to Kulyab (section Daraiob Pass), and at a military training site close to Kulyab (sections Karanak Crook and Cantaloupe).

We selected these sections to assemble a standard section of the Upper Cretaceous-Neogene strata and to investigate lateral variations within individual lithostratigraphic units using existing 1:200,000 geologic

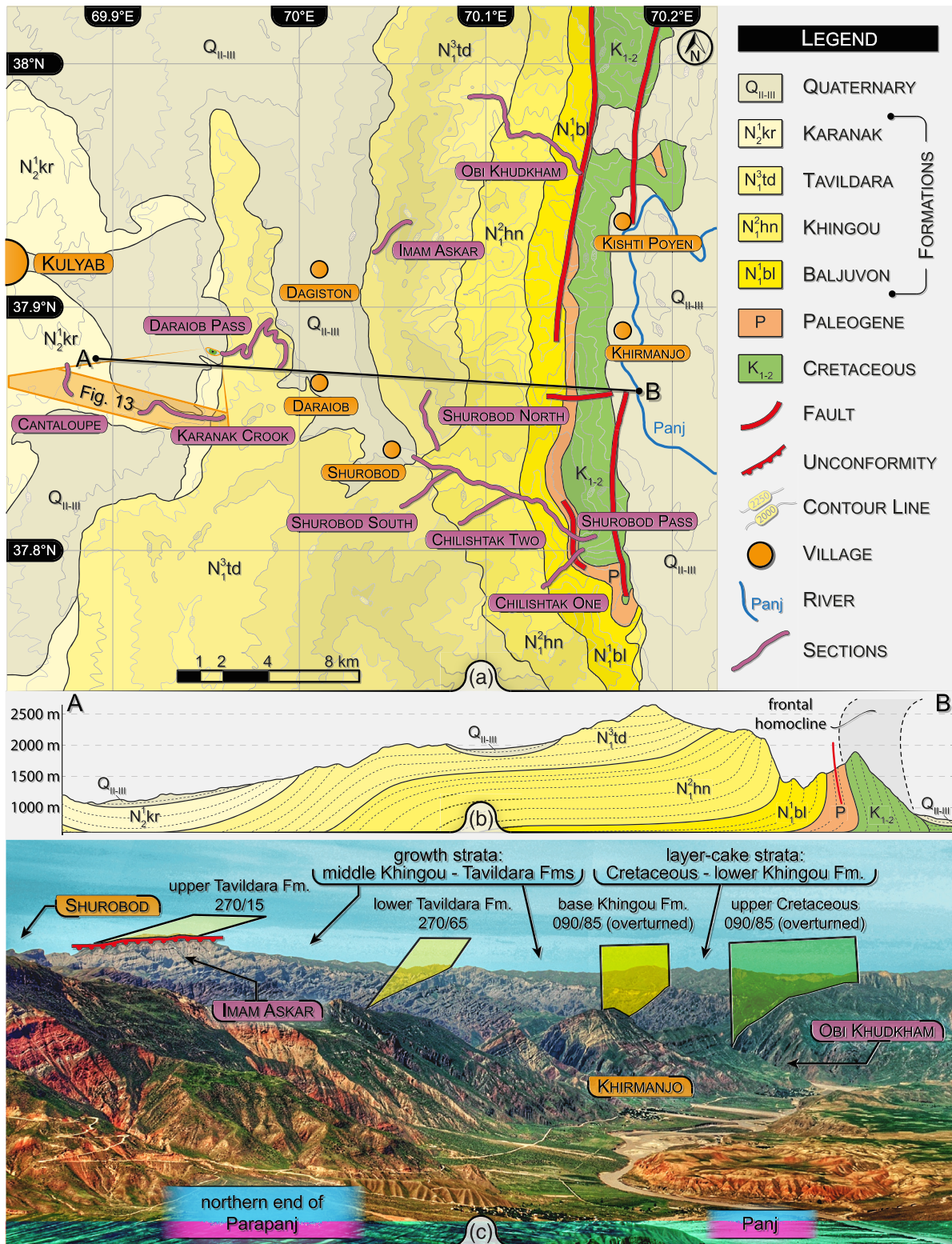


Figure 2. (a) Geologic map of the eastern margin of the Tajik basin abutting on the western spur of the Pamir. Studied sections are marked. (b) Simplified cross sections A and B in (a) highlighting the major structures and the growth strata in stratigraphic units N₁²hn and N₁³td (Khingou and Tavildara Formations). (c) View toward NW along the Panj and Parapanj valleys. The eastern Tajik basin exposes Cretaceous to lower Miocene layer-cake strata followed by middle-upper Miocene growth strata and a Miocene angular unconformity exposed around Imam Askar. Planes illustrate declining dips from older to younger strata.

Table 1
Stratigraphic Units and Their Thickness

Stage	Epoch	Formation	Member	Thickness (m)
Synorogenic	Pliocene	Karanak		1,200
		Tavildara		1,500–2,300
	Miocene	Khingou		1,100–1,600
		Baljuvon (total)		800–1,100
		Baljuvon	Childara	250–600
		Baljuvon	Kamolin	120–300
Preorogenic	Oligocene	Baljuvon	Shurisay	300–400
	Eocene	Sumsar		50
		Isfara-Hanabad		15
		Rishtan		—
		Turkestan		—
		Alai		70
		Suzak		12
	Paleocene	Bukhara		50
		Akdjar		130
	Late Cretaceous	undifferentiated		275

maps (GRI, 1961–1965; see Text S1 in the supporting information) and our own mapping. We logged these sections and studied their three-dimensional sedimentary architecture. For the reconstruction of flow directions, we recorded the dips of imbricated clasts and fore-sets of cross-bedded strata and the plunge of scour lineations; measurements of at least 20 imbricated clasts per conglomerate bed and at least three fore-set dips were averaged. We corrected all flow directions for structural tilt and describe all spatial relations with regard to their present orientation, since the precise timing of the paleomagnetically determined rotations is unknown (Pozzi & Feinberg, 1991; Thomas et al., 1994). We sampled sandstones, representing distinct lithofacies types (LFTs) of bed load, and analyzed their granulometry and modal composition in thin sections and polished slabs. We used the Gazzi-Dickinson method for the quantification of the modal composition, counting at least 400 grains per thin section, to minimize the dependence of rock composition on grain size (Dickinson, 1970; Gazzi, 1966; Ingersoll et al., 1984). We analyzed mudstones and siltstones, representing the fine-grained lithofacies of suspension load, for variations in the major oxides and trace elements; these were measured at ALS Global (Loughrea, Ireland) with X-ray fluorescence and inductively coupled plasma mass spectroscopy. Table 1 summarizes the studied stratigraphic units and their thicknesses, and Table 2 provides the descriptions and interpretations of the observed LFTs. Table S1 in the supporting information lists the geochemical data, and Table S2 provides correlations between various geochemical data.

3. Late Cretaceous-Neogene Stratigraphy

The strata of the Tajik basin are classically subdivided into preorogenic and synorogenic stages based on their depositional character (Figures 3 and 4; e.g., Hamburger et al., 1992; Leith, 1982; Nikolaev, 2002). The preorogenic stage encompasses <5-km-thick Upper Triassic-Jurassic to Paleogene shallow marine to fine-grained clastic continental deposits; in the Shurobod area, the Upper Cretaceous-Paleogene preorogenic deposits—studied herein—are ~600 m thick (Table 1). The basal décollement of the Tajik fold-thrust belt of the Afghan-Tajik depression lies within the Kimmeridgian-Tithonian evaporites (e.g., Gubin, 1960; Leith et al., 1981). Biostratigraphy and partly magnetostratigraphy provide a firm control on the age and lateral correlation of the Jurassic, Cretaceous, and Paleogene basin-wide marine strata (Bosboom et al., 2013, 2015; Chapman et al., 2019; Dzhililov et al., 1982; Kaya et al., 2019). In contrast, the chronostratigraphic classification of the Neogene synorogenic deposits is controversial. These continental, in general, coarse-grained clastic deposits vary laterally throughout the Tajik basin and were dated and correlated by lithostratigraphic similarities and spore and pollen assemblages (Dzhililov et al., 1982). Ostracods and rare vertebrate remains provide accurate but isolated age control (e.g., Forsten & Sharapov, 2000). The Neogene succession is 5.2–7.5 km thick in the eastern part of the basin (Table 1; Kondur et al., 1974; Dzhililov et al., 1982).

Table 2
Description and Interpretation of Lithofacies Types (LFTs) of the Shurobod Area in the Eastern Tajik Basin

Name	Code	Facies	Description	Contacts	Interpretation
LFT 1	Gmg	Cobble-boulder conglomerates, matrix-supported	Inversely to normally graded, poorly sorted conglomerates, matrix-supported, matrix poorly sorted, clasts sub-rounded to angular, outsized clasts up to 400 cm	Base flat, non-erosional; top gradational to LFTs 2 and 3	Pseudo-plastic debris flows (viscous)
LFT 2	Gmm	Pebble-cobble conglomerate, matrix-supported	Disorganized, poorly sorted conglomerates, matrix-supported, matrix poorly sorted, clasts rounded to angular	Base non-erosional, gradational to LFT 1; top gradational to LFTs 3 and 5	Plastic debris flow
LFT 3	Gcm	Pebble-cobble conglomerate, clast-supported	Disorganized, densely packed, poorly to moderately sorted conglomerates, clast-supported, matrix sorting poor to moderate, nests of imbricated particles, clasts rounded to angular	Base mostly non-erosional or gradational to LFT 1	Hyper-concentrated flows
LFT 4	Gh	Pebble-cobble conglomerate, clast-supported, imbricated	Organized, moderately sorted conglomerates, matrix sandy, moderately to well sorted, imbrication common, faint horizontal stratification, clasts rounded to sub-rounded, elongated	Base undulatory and erosive; top gradational to LFT 10	Longitudinal bedforms; channel fills
LFT 5	Gm	Granule-pebble conglomerate, matrix-supported	Normally or inversely graded, well sorted conglomerates, matrix-supported, mud-rich matrix, clasts sub-rounded to angular	Base sharp and non-erosive; top sharp or gradational to LFT 8	Mud flows (viscous)
LFT 6	Gt	Granule-pebble conglomerate, trough cross-bedded, clast-supported	Organized, normally graded, well sorted conglomerates, clast-supported, trough cross-stratification	Base sharp and erosional; top gradational to LFT 7	Transverse bedforms
LFT 7	St	Sandstone, cross-bedded	Tabular to trough cross-bedded, subordinately horizontally bedded medium to coarse sandstones	Base erosional or gradational to LFT 6; top sharp or gradational to LFTs 9, 10, and 12, occasional bioturbation	Waning-stage channel and bar-top deposits
LFT 8	Sm	Sandstone, massive	Massive, medium, coarse to granular sandstones, floating pebbles	Base sharp or gradational to LFT 5	Sandy mud flows
LFT 9	Sr	Sandstone, ripple-bedded	Ripple-bedded fine- to medium-grained sandstones, occasionally glauconite-bearing	Base sharp or gradational to LFT 7; top gradational to LFT 10	Lower flow regime, bedload, partially wave-induced
LFT 10	Sh	Sandstone, horizontally bedded	Horizontally bedded fine- to coarse-grained sandstones, often fining upward	Base sharp or gradational to LFTs 4 and 7; top sharp or gradational to LFTs 9 and 12	Lower flow regime, waning flow deposit
LFT 11	Sil	Marl, laminated	Laminated to massive marls, grayish, highly calcareous, bioturbation, fossiliferous	Base sharp	Carbonate mud settling in water-column, marine
LFT 12	Sih	Siltstone, horizontally bedded	Laminated siltstones, red, partly bioturbation, rootlets, bleaching halos	Base sharp or gradational to LFT 7; top sharp	Floodplain fines, suspension settling from shallow water column
LFT 13	Cc	Carbonates	Massive to nodular, sparitic to micritic carbonates, fossiliferous	Base mostly sharp	Carbonaceous shallow marine deposits
LFT 14	Gy	Gypsum, anhydrite	Layers, nodules and veins of precipitated gypsum and anhydrite deposits intercalated with LFT 12	Base and top sharp	Playa/sabkha precipitate
LFT 15	Pc	Carbonate crusts	Carbonaceous nodules and crusts intercalated with LFTs 10 and 12	Base fuzzy to gradational; top sharp	Immature calcisol

		GSS	RSS	LSS	LSS*	LSS**	LSS***	this study		
Neogene	Pliocene	L Piacenzian (2.58)	Kuljab	Polizak	Kuruksai	not considered	not considered	(disconformity)		
		E Zanclean (3.600)	Polizak	Karanak	Polizak			Karanak		
		Messinian (5.333)	Tavildara	Tavildara	Karanak			(disconformity)		
	Miocene	L Tortonian (7.246)	Kafirigan	Kafirigan	Tavildara			Tavildara	Tavildara	
		M Serravallian (11.63)	Khingou	Khingou	Khingou			Khingou	Khingou	
		E Langhian (13.82)	Baljuvon	Childara Kamolín	Childara Kamolín			Childara Kamolín	Childara Kamolín	
		E Burdigalian (15.97)								
		E Aquitanian (20.44)								
	Paleogene	Oligocene	L Chattian (28.1)	Shurisay	Baljuvon			Shurisay	Baljuvon	Shurisay
			E Rupelian (33.9)					Hissarak	Hissarak	Hissarak
Eocene		L Priabonian (37.8)	Sumsar	Sanglak Kushan	Sumsar	Sumsar	Sumsar			
		M Bartonian (41.2)	Isfara-Hanabad	Tochar II	Isfara-Hanabad	Isfara-Hanabad	Isfara-Hanabad			
		E Ypresian (47.8)	Rishtan	Tochar I	Rishtan	Rishtan	Rishtan			
		Lutetian (56.0)	Turkestan	Beshkent	Turkestan	Turkestan	Turkestan			
		E Ypresian (47.8)	Alai	Jukar	Alai	Alai	Alai			
Paleocene		L Thanetian (59.2)	Suzak	Givar	Suzak	Suzak	Suzak			
		M Selandian (61.6)	Bukhara	Karatag Aruktau Tabakcha	Bukhara	Bukhara	Bukhara			
		E Danian (66.0)	Akdjar	Akdjar	Akdjar	Akdjar	Akdjar			

Figure 3. Cenozoic stratigraphic subdivisions. Global stratigraphic scale (GSS; Cohen et al., 2013; numerical ages in Ma according to Gradstein et al., 2012); regional stratigraphic scale (RSS; Vjalov, 1940; Simakov, 1952; Kreydenkov & Raspopin, 1972; Vlasov et al., 1991; Nikolaev, 2002); local stratigraphic scale (LSS; Davidzon et al., 1982; Dzhililov et al., 1982); alternative local stratigraphic scales: LSS*—Forsten and Sharapov (2000); LSS**—Kaya et al. (2019) with timing of Paleogene incursions; LSS***—synthesis of Carrapa et al. (2015) with date of volcanic ash bed and Chapman et al. (2019) with detrital zircon fission-track ages, considered maximum depositional ages for the formations. The right column shows the subdivision into preorogenic and synorogenic stages and timing of formations adopted in this paper. The \leq ~Ma notation in the LSS*** and “this study” columns highlight that the ages given for the Formation/Member boundaries are maximum ages.

Assorting the sedimentary deposits into the established stratigraphic formations (subsequently abbreviated as Fm) is complicated by the existence of several classification schemes, especially for the better-dated preorogenic stages (Figure 3). The synorogenic stages have been described more consistently; however, opinions diverge on the age of the Fm boundaries (Dzhililov et al., 1982; Forsten & Sharapov, 2000; Nikolaev, 2002). Although a local stratigraphic scale (LSS; Figure 3) for the Tajik basin exists (Davidzon et al., 1982; Dzhililov et al., 1982), we utilized the regional stratigraphic scale to facilitate future research, as the regional stratigraphic scale appears in the geologic map of western Central Asia (Vlasov et al., 1991). We use the Member subdivision of the LSS for the Baljuvon Fm, as it best reflects the observed subdivision of genetically linked deposits in the Shurobod area (Table 1 and Figure 3).

In the studied sections, the preorogenic strata comprise the Late Cretaceous to Paleogene epochs (Table 1), with parts of the middle and late Eocene missing (Figure 4). The exposed synorogenic deposits span the Oligocene-early Pliocene. The first formation signaling tectonic activity—the Oligocene Baljuvon Fm—comprises the Shurisay, Kamolín, and Childara Members (Figures 3 and 4), as the Rupelian Hissarak Beds are documented only in the northern part of the Tajik Basin (Dzhililov et al., 1982). The overlying Khingou and Tavildara Fms were classified as Miocene (Vlasov et al., 1991). The Karanak Fm—assigned to the early Pliocene—constitutes the uppermost preserved synorogenic deposits in the Shurobod area.

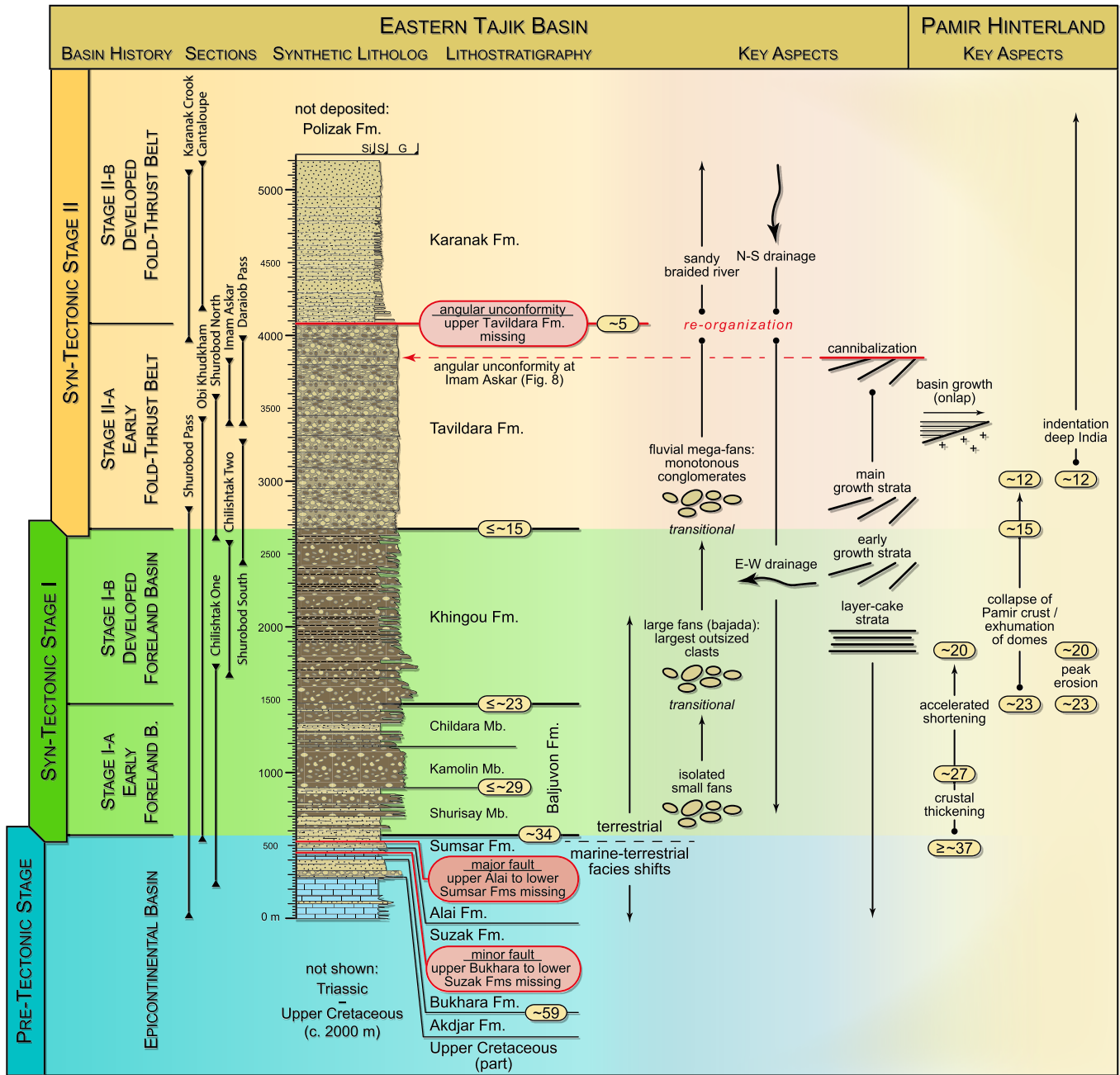


Figure 4. Basin development and synthetic standard section of the eastern Tajik basin and correlation with tectonic evolution of the Pamir hinterland. The \leq ~Ma notation highlights that the ages given for these Formation/Member boundaries are maximum ages.

Carrapa et al. (2015) calibrated intervals of marine Paleogene strata in the northern Tajik basin to the Ypresian and the Bartonian-early Priabonian, respectively; the changeover from marine to nonmarine strata yielded a volcanic ash layer, dated geochronologically at ~39 Ma (Figures 1c and 3). Unfortunately, they did not provide an assignment to specific Formations, neither for the biostratigraphic data nor the geochronologic age. Based on biostratigraphic and magnetostratigraphic data, Kaya et al. (2019) calibrated the three Paleogene incursions of the Turan Sea into the Tarim and Tajik basins, corresponding to the transgressions 3–5 sensu Bosboom et al. (2013, 2015). During the first incursion (~59–52 Ma, late Thanetian-early Ypresian), the interval of the Tabakcha to lower Jukar Fms was deposited in the northern Tajik Basin;

this interval corresponds that of the Bukhara to lower Alai Fms in the eastern Tajik basin (Figure 3). The second incursion (~47–41 Ma, Lutetian-early Bartonian) comprises the upper Jukar-Tochar I Fms in the northern Tajik basin, corresponding to the Turkestan Fm in the eastern Tajik basin. The third and final incursion (~40–37 Ma, late Bartonian-early Priabonian) comprises the Tochar II-Hissarak Fms in the northern Tajik basin, corresponding to the Isfara-Hanabad Fm in the eastern Tajik basin. Thus, the lower interval of marine strata of Carrapa et al. (2015) seems to correspond to the first incursion of Kaya et al. (2019), and the marine interval including the ~39-Ma age marker probably corresponds to the second incursion of Kaya et al. (2019). As addressed by Bosboom et al. (2015), the ~39-Ma age marker of Carrapa et al. (2015) does not correspond to the final incursion.

Accepting these age constraints, we used the following ages to calibrate the Paleogene strata in the eastern Tajik basin (Figure 3). The base of the Bukhara Fm corresponds to the onset of the first incursion (~59 Ma) and the lower Alai Fm relates to the first regression (~52 Ma). The second transgression (~47 Ma) is correlated with the upper Alai Fm, and the second regression—dated at ~39 Ma (Carrapa et al., 2015)—is correlated with the top of the Turkestan Fm. As the onset of the third incursion—~40 Ma according to Kaya et al. (2019)—predates the second regression, dated at ~39 Ma (Carrapa et al., 2015), no reliable age is available for the base of the Isfara-Hanabad Fm so far. The top of this formation is correlated with the third regression (~37 Ma).

Chapman et al. (2019) reported detrital zircon fission-track age populations from samples of the synorogenic Formations in the Dashtjum section, located in the eastern Tajik basin a few kilometers to the north of our study area (Figure 1c). They interpreted the ages from the Kamolin Member (~29–27 Ma) of the Baljuvon Fm, Khingou Fm (~23–18 Ma), and basal Tavildara Fm (~15 Ma) to represent hinterland exhumation/cooling ages, and thus as maximum depositional ages for the Members/Formations, in which they were sampled; they argued for a short lag time between exhumation, erosion, and deposition. Abdulhameed et al. (2020) reported a comparable detrital apatite fission-track age (~25 Ma) for the basal Khingou Fm in the north central Tajik basin. Accordingly, we used the detrital zircon fission-track ages reported by Chapman et al. (2019) as maximum ages for the synorogenic Fms (Figure 3).

Klocke et al. (2017) described the Oligocene-Pliocene synorogenic deposits of the Tajik basin ~100 km north of our working area (Figure 1c). They documented a first phase of synorogenic conglomerate deposition derived from the south—the Pamir—in the Kamolin Member of the Baljuvon Fm, followed by a period of reduced sediment supply in the Childara Member. Overlying sandstones and conglomerates of the likely early-middle Miocene to Pliocene Khingou, Sary Ob, Tavildara, and Karanak Complexes onlap the Paleozoic basement of the North Pamir, indicating growing hinterland topography. Their likely middle-upper Miocene Sary Ob Complex, representing the top and base of the Khingou and Tavildara Fms, respectively, is bounded by unconformities and growth strata. Within the middle Miocene-lower Pliocene Tavildara and Karanak Fms, sediment-transport directions, deflected to the southwest, indicate emerging basin topography, establishing the modern drainage pattern.

4. Results: Stages of Basin Evolution in the Shurobod Area

The strata in the Shurobod area record the preorogenic stage, the period prior to the onset of the effects of the uplift of the Pamir, and the synorogenic stage, the formation of a foreland basin and its transformation into a fold-thrust belt (Figure 4). These stages show distinct sedimentation rates and depositional environments. Discrete stratigraphic intervals exhibit large-scale stratal pattern architecture and basin morphology. The investigated preorogenic stage spans the succession from the Late Cretaceous to the top of the late Eocene Sumsar Fm. An initial stage of synorogenic foreland-basin formation commenced in the Oligocene Baljuvon Fm; the foreland basin was fully established in the early Miocene Khingou Fm. The middle Miocene-Pliocene Tavildara, Karanak, and Polizak Fms represent the late synorogenic fold-thrust belt formation stage.

4.1. Preorogenic Stage: The Epicontinental Basin

4.1.1. Description

The investigated Upper Cretaceous-upper Eocene preorogenic strata exposed in the Shurobod Pass and Obi Khudkham sections (Figure 2) are ~600 m thick. At Shurobod Pass, the middle-late Eocene Fms—the upper

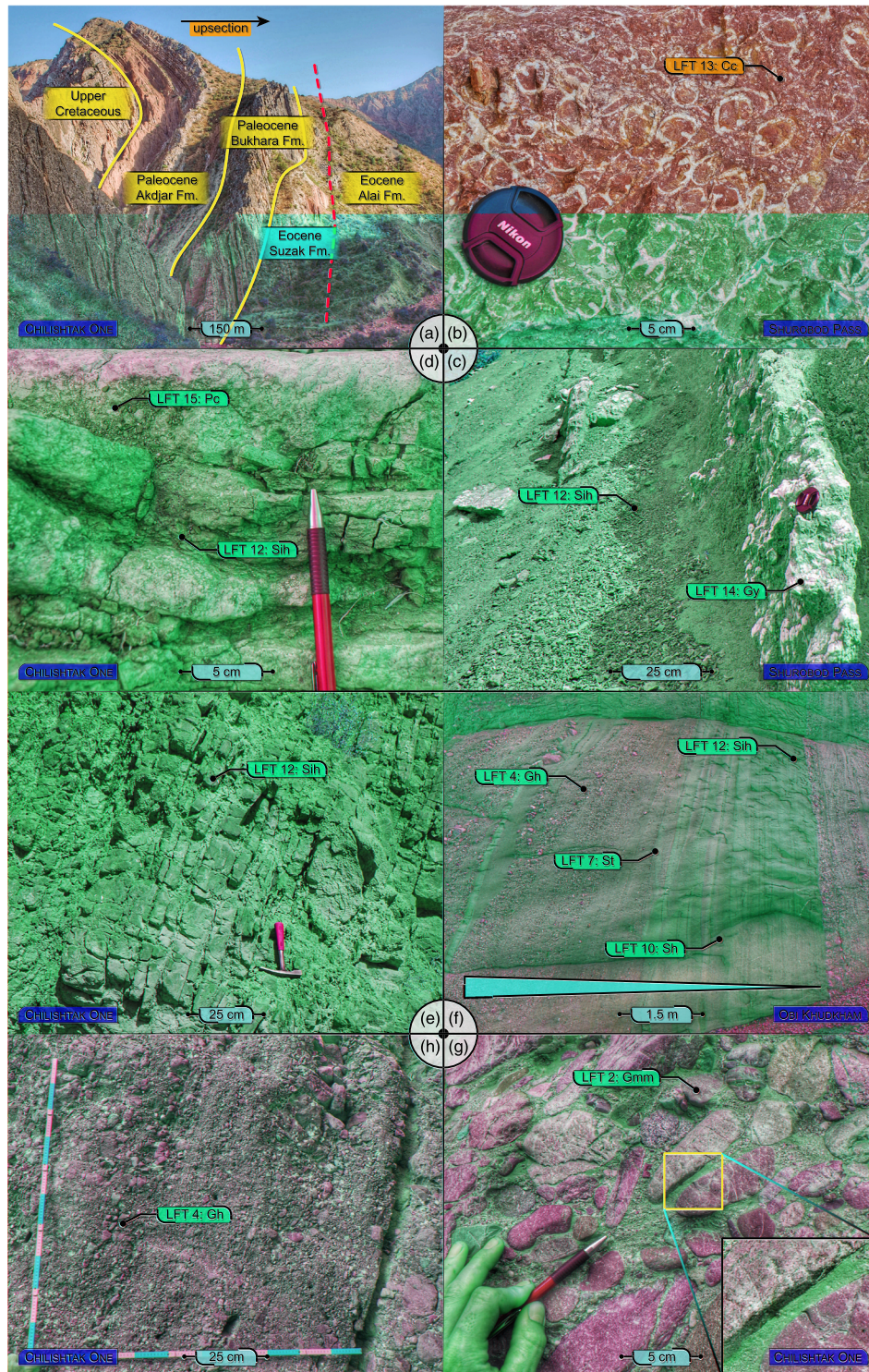


Figure 5. Field examples and lithofacies (LFT; Table 2) of the (a–d) preorogenic, Cretaceous-Paleogene and (e–h) early synorogenic, Oligocene (Baljuvon Formation) strata. (a) Cretaceous-Eocene strata, Chilishtak One section; the red dashed line marks a minor fault between the Bukhara and Suzak Fms. (b) Colonies of rudist bivalves (Hippuritoidae), uppermost Cretaceous strata, Shurobod Pass section. (c) Oxidized reddish siltstones with intercalated, ~20-cm-thick gypsum crusts, Paleocene Akdjar Formation, Shurobod Pass section. (d) Pedogenic siltstones transitioning into calcrete incrustation, Eocene Alai Formation, Chilishtak One section. (e) Massive to horizontal-laminated siltstones of the Shurisay Beds, Baljuvon Formation, Chilishtak One section. (f) Upward fining pebbly conglomerate-sandstone successions followed by horizontal-laminated siltstone, Shurisay Member, Baljuvon Formation, Obi Khudkham section. (g) Clayey to sandy matrix in a poorly sorted, densely packed conglomerate of the Kamolin Member, Baljuvon Formation, Chilishtak One section. (h) Faintly stratified, clast-supported conglomerate of the Kamolin Member, Baljuvon Formation, Chilishtak One section.

Alai, Turkestan, Rishtan, Isfara-Hanabad, and lower Sumsar Fms—are tectonically buried by the Upper Cretaceous and Paleogene rocks up to the lower Alai Fm (Figure 5a). At Obi Khudkham, ~65 m of upper Eocene strata—the upper Isfara-Hanabad and Sumsar Fms—are exposed. Correlations with the neighboring regions (GRI, 1961–1965) indicate that an ~350-m-thick section (middle Eocene; the upper Alai, Turkestan, Rishtan, and lower Isfara-Hanabad Fms) is missing; therefore, the Upper Cretaceous-Eocene strata may have been ~950 m thick. Above the Lower Cretaceous terrestrial siliciclastic rocks, marine carbonates dominate the ~275-m-thick Upper Cretaceous succession. The Cenomanian has shallow marine limestone and sandstone, the Turonian dark shale, the Coniacian-Santonian cyclic limestone-marl alternations, and the Campanian-Maastrichtian shallow marine limestones and rare evaporates. In the Shurobod Pass section, the Coniacian-Maastrichtian strata contain bivalves, ammonites, gastropods, brachiopods, corals, and shark teeth. In their upper part, repeated pro-gradations and retro-gradations of marine clastic rocks culminated in ≤10-m-thick, calciferous, fine- to medium-grained, partly pebbly sandstones. These graywackes contain pebbles composed of quartz, sedimentary, and igneous clasts. At the top, a prominent, ~15-m-thick, reddish brown limestone—characteristic for all studied sections—has colonies of rudists (Figure 5b).

The ~130-m-thick Akdjar Fm comprises transitional marine to terrestrial deposits. At its lower part, bioturbated red-brown mudstone and sandstone overlie rudist limestone. The middle and upper parts have ≤40-m-thick stratified gypsum and pedogenic reddish mudstones and siltstones with numerous ≤2-m-thick gypsisols (Figure 5c). The Shurobod Pass section has an ~55-m-thick oligomict, matrix- to clast-supported conglomerate in the middle Akdjar Fm. Red-brown, shaly to sandy, calciferous matrix supports ≤30-cm-long angular limestone, quartz, and quartzite clasts. This is overlain by up to 50 m of Bukhara-Fm limestone, which forms a ridge that outlines the west facing anticline of the Shurobod Pass section (Figure 5a). The lower and upper parts comprise alternating gray to black marl and limestone, partly rich in plant fragments, and ≤2-m-thick limestone beds, respectively. The top of the Bukhara Fm has nodular limestone grading into ~12-m-thick, grayish-green marl intercalated with oyster-bearing limestone and glauconitic sandstone of the lower Suzak Fm. Its upper part is tectonically buried and exposure continues with ~7-m-thick gray marls and coquina beds of the lower Alai Fm. The upper Alai Fm has ~65-m glauconitic sandstone and reddish to red-brown, partly mottled (pedogenic) mudstones and siltstones (Figure 5d). At Shurobod Pass, the upper Alai to lower Sumsar Fms are tectonically buried. At Obi Khudkham, the exposure continues with the ~15-m-thick, red-brown, glauconitic sandstones and siltstones of the upper Isfara-Hanabad Fm. The overlying Sumsar Fm comprises ~50-m-thick, monotonous red-to-red-brown, horizontal-laminated and trough-cross bedded siltstones and sandstones with a pedogenic overprint.

4.1.2. Depositional Environment

The change from terrestrial Lower Cretaceous to marine Upper Cretaceous deposits corresponds to a global sea-level rise (Haq et al., 1987; Vail & Mitchum, 1979). This transgression incorporated the Tajik basin into a shallow-marine carbonate shelf, stretching from the Turan Sea across Central Asia into the Tarim basin (e.g., Popov et al., 2004). Repeated progradation of coastal clastic rocks—≤10-m-thick, calciferous sandstones, particularly well exposed in the Shurobod Pass section—indicates Late Cretaceous shallowing. The Paleogene succession records repeated changes from red beds of coastal plains and sabkhas to shallow marine shelf and inland seas (Bosboom et al., 2015; Popov et al., 2004). The marine limestones, marls, and shales of the Bukhara-lower Alai Fms; the marine shales and marls of the Turkestan Fm; and the marine shales and marls of the Isfara-Hanabad Fm correspond to the three incursions described by Bosboom et al. (2015) and Kaya et al. (2019). Red beds record regressions in the Akdjar, the middle Alai, and the Rishtan Fms. From the latest Eocene onward, a coastal plain persisted.

4.1.3. Sedimentation Rate, Stratal Pattern Architecture, and Basin Type

The ~32-Myr duration and ~675-m thickness of the early Paleocene to late Eocene Fms approximate an apparent sedimentation rate of ~20 m/Myr; this rate—as all sedimentation rates calculated herein—do not include compaction and possible intervening erosion episodes. The Paleogene Fms have a layer-cake architecture with uniform lithofacies and thickness (Dzhalilov et al., 1982). The hundreds-of-kilometer-broad facies belts imply shallow facies gradients. The large areal fluctuations of the Paleogene sea indicate inundated lowlands without significant morphology. The low sedimentation rate and the layer-cake architecture suggest an epi-continental basin.

4.2. Synorogenic Stage I: Foreland Basin

Increased strata thickness and onset of conglomerate deposition in individual sections of the sandstone-dominated Baljuvon Fm (~34–23 Ma) and the conglomerate-dominated Khingou Fm (\leq ~23–15 Ma) herald the synorogenic stage I (Figure 3). These Fms document two stages in the evolution of the eastern Tajik basin (Figure 4).

4.2.1. Substage Ia: Early Foreland Basin—Formation of Local Alluvial Fans

4.2.1.1. Description

The Baljuvon Fm comprises brick-red sediments: ~800 m thick at Shurobod Pass, ~1,100 m thick at Obi Khudkham, and ~900 m thick at Chilishtak One. Thus, it is much thicker than the Paleogene section. The Shurisay Member—assigned to the early Oligocene (Figure 3)—shows uniform lithology from south to north (Figure 6a); is 300–400 m thick; and composed of shale, siltstone, and sandstone (Figure 5e) with occasional centimeter- to decimeter-thick conglomerate beds. These granule- to pebble-sized, mainly clast-supported conglomerates (LFT 6; Table 2) have scoured bases and internal cross bedding. Incised conglomerate beds have sharp tops and taper out laterally within decimeters to meters. Nonincised conglomerates are tabular and gradational with overlying sandstones (Figure 5f). At Shurobod Pass, matrix-supported conglomerates (LFT 5) occur. Horizontally laminated and cross-bedded, mostly tabular and laterally persistent lithofacies (LFTs 7, 10, and 12) characterize the finer-grained lithologies. Pedogenesis, indicated by rootlets and in situ brecciating (Figure 6a), has particularly affected the deposits of the Obi Khudkham and Chilishtak One sections.

The 120- to 300-m-thick Kamolin Member—assigned to the early to late Oligocene (Figure 3)—shows lithofacies differences from south to north (Figure 6a). In the Chilishtak One section, the Kamolin Member has ~280 m of conglomerates, composed of 2- to 20-m-thick amalgamated, matrix- to clast-supported packages (LFTs 2 and 3) with only faint bedding. A reddish clayey to sandy, poorly sorted matrix supports angular to subrounded clasts (Figure 5g) with 3- to 10-cm average and 10- to 60-cm maximum particle size (MPS). While fine-clastic interbeds are missing at Chilishtak One, 2- to 20-m-thick conglomerates and 0.5- to 5.0-m-thick shales, siltstones, and sandstones occur at Shurobod Pass and Obi Khudkham. The pebble- to cobble-sized conglomerates are clast supported and show horizontal- to low-angle cross-bedding (Figure 5h). Locally, conglomerates, sandstones, and siltstones (LFTs 4, 6, 7, 10, and 12) form 5- to 10-m-thick fining upward successions.

The 250- to 600-m-thick Childara Member—assigned to the late Oligocene (Figure 3)—resembles the Shurisay Member. Up to 100-m-thick shales, siltstones, and sandstones (LFTs 10 and 12) are intercalated with 2- to 15-m-thick conglomerates (LFTs 2, 3, 5, and 6); the fine-grained lithofacies shows pedogenic features, that is, rootlets and destruction of bedding structures. Thicker matrix- to clast-supported conglomerates, with 5–30 cm MPS, are composed of amalgamated 1- to 3-m-thick, occasionally low-angle to planar cross-bedded sheets (Figure 6a). The lateral variations between the sections are minor. The lower part of the Childara Member is fine grained and becomes coarser toward the top at Shurobod Pass and Chilishtak One. There, the boundary to the Khingou Fm is transitional. Immature calcsols in the uppermost Childara Member occur at Chilishtak One and Obi Khudkham.

4.2.1.2. Depositional Environment

During the early Oligocene, the coastal plain in the eastern Tajik Basin changed into a distal alluvial plain environment traversed by few fluvial channels. Paleocurrent measurements indicate grossly west-directed (present coordinates) transport (Figure 6a). The fine-clastic red beds of the Shurisay Member were deposited on extensive floodplains with alternating sedimentation and subaerial exposure, promoting pedogenesis (Jones et al., 2011; McPherson, 1979). Erosive and laterally restricted conglomerates are channel deposits of confined flows incised into the floodplain fines. Nonerosive, laterally consistent conglomerates and sandstones are unconfined subaerial flow deposits, indicating flood stages with increased sediment supply (Colombera et al., 2013; Gibling, 2006). In the early to late Oligocene, a basinward progradation of proximal alluvial sediments caused a major change of the depositional environment. The stacked debris and hyper-concentrated flows of the Kamolin Member formed isolated conglomerate packages with sharp and tabular bases and convex-up tops. These bodies are up to a few kilometer across and transition laterally into distal debris flows, mudflows, and sheetsands with floodplain fines. The red-bed facies (LFTs 7, 10, and 12) of the lower Childara Member indicate the return to a distal alluvial plain, characterized by alternating

CHILSHATAK ONE

sedimentation and nonsedimentation. The gradual increase of coarse clastic sediments (LFTs 2, 5, and 8) in the upper Childara Member indicates a transition into a medial to proximal alluvial plain of a prograding fan system in the hinterland.

4.2.1.3. Sedimentation Rate, Stratal Pattern Architecture, and Basin Type

The ~11-Myr duration (Oligocene) and the ~950-m thickness of the Baljuvon Fm approximate an apparent sedimentation rate of ~86 m/Myr. Variable sediment thickness and changing lithofacies imply locally different sedimentation rates and thus the development of a moderate morphology. The advance of alluvial fans in the Kamolin Member marks the onset of synorogenic deposition with thicker, more amalgamated, and coarser conglomerates at section Chilishtak One in the south of the Shurobod region. The increased sedimentation rate and the developing basin morphology suggest a transformation of the epicontinental basin into a foreland basin in the Oligocene.

4.2.2. Substage Ib: Developed Foreland Basin—Coalescence of Alluvial Fans

4.2.2.1. Description

The violet-colored clastic rocks of the early Miocene (Figure 3) Khingou Fm are ~1,200 m thick at Shurobod Pass and ~1,600 m thick at Obi Khudkham. At Chilishtak Two, the ~960-m-thick lower part, and at Shurobod South, the topmost ~100 m are exposed (Figures 2 and 6b). The Khingou Fm has meter- to decameter-thick packages of conglomerate intercalated with decimeter- to meter-thick violet or brick-red siltstone and sandstone. In the lower Khingou Fm at Chilishtak Two and Shurobod Pass, 1- to 3-m-thick, unstratified beds of cobble- to boulder-sized, matrix- to clast-supported conglomerate (Figure 7a; LFTs 1, 2, and 3) have nonerosive to weakly erosive bases and form 4- to 40-m-thick, stacked tabular units. Clast size varies within individual beds forming both coarsening-upward as well as fining-upward sets (Figures 7b and 7c). The angular to subrounded clasts have an average size of 5–20 cm and 20–80 cm MPS (Figure 7c); out-sized 100- to 400-cm clasts also occur (Figure 6b). At Obi Khudkham, the lower to middle Khingou Fm shows monotonous, ≤50-m-thick, tabular packages of conglomerate intercalated with decimeter- to meter-thick, brick-red siltstone (Figure 7d; LFT 12). The siltstones are stacks with 1- to 2-m-thick beds of matrix- to clast-supported conglomerate (LFTs 2 and 3), showing an average clast size of 3–12 cm and 60–90 cm MPS (Figure 6b); the clasts are angular to subrounded. The conglomerate matrix is silt- to pebble-sized. Vertical variations in clast size, matrix sorting, and matrix composition of the conglomerates are minor (Figure 7e).

In the middle part of the Khingou Fm at Shurobod Pass and Chilishtak Two, stacked conglomeratic packages are decimeter- to meter-thick, faintly stratified, and clast-supported (LFT 3) with an average clast size of 1–8 cm and a poorly sorted, clayey to sandy matrix. Clasts are subangular to subrounded, partially elongate, and occasionally form imbricated nests. The particle size decreases gradually toward the tops of individual beds. At the top of the middle Khingou Fm, the conglomerates are decimeter-thick, red-violet, and matrix-supported (LFT 5). The angular to subrounded clasts range from pebble-size to granule-size and float in a clayey-silty matrix. The fine-grained conglomerates grade occasionally into massive red-violet sandstones (LFT 8) and are overlain by decimeter-thick, red-brown siltstones (LFT 12). The base of the fine- and coarse-clastic lithofacies is dominantly nonerosive, but occasional basal scours occur. At Obi Khudkham, the lithofacies of the middle Khingou Fm is comparable to its lower part. Generally, the sediment packages become increasingly wedge-shaped over lateral distances of hundreds of meters and less uniform compared to the lower Khingou Fm. As a result, the near-vertical dip angles of the strata decrease steadily upsection (Figure 2b).

The lithofacies of the upper Khingou Fm at Shurobod Pass and Shurobod South consists of 10- to 60-m-thick, amalgamated conglomerates (LFTs 2, 3, 4, and 5), intercalated with decimeter- to meter-thick, brick-red to violet siltstones and sandstones (Figure 7f; LFTs 7, 10, and 12). The conglomerates are matrix- to clast-supported with an average clast size of 1–8 cm and 10–20 cm MPS (Figure 6b). Overlying 1- to 5-m-thick, brick-red to violet, granule, matrix-supported conglomerates (LFT 5) alternate sharply with 1- to 15-m-thick violet, pebbly, clast-supported conglomerates (LFTs 3, 4). The matrixes of both conglomerate types are sandy and moderately to well sorted. Basal contacts of the clast-supported conglomerates are increasingly erosive toward the top, and the conglomeratic units show higher lateral variability than in the lower and middle Khingou Fm. The finer-grained lithologies are mainly represented by horizontal-laminated and cross-bedded, brick-red to violet siltstones and sandstones (LFTs 7, 10, and 12), which alternate with the matrix-supported conglomerates. Modifications of the siltstones and sandstones

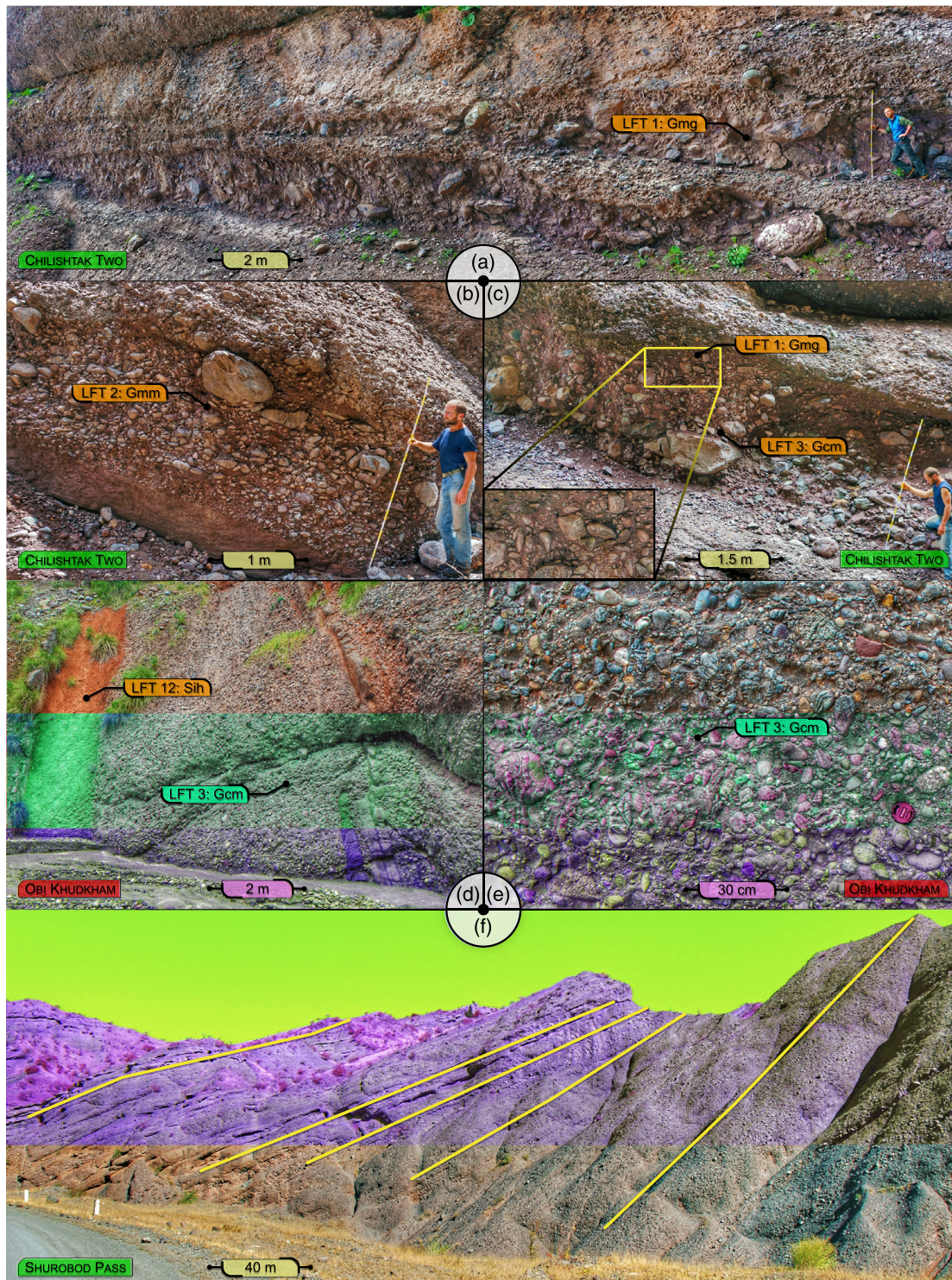


Figure 7. Field examples and lithofacies (LFT; Table 2) of the Khingou Formation. (a) Sheet-like conglomerate beds with sharp base and convex-up tops with cyclic upward fining boulders to cobbles occur within 10- to 20-m-thick units. Maximum particle size (MPS) is ~29 cm; outsized clasts are ~1.5 m; Chilishtak Two section. (b) Tabular, ~1.6-m-thick, inversely graded and matrix-supported conglomerate, MPS is ~26 cm, outsized clasts are up to 75 cm; Chilishtak Two section. (c) Tabular, ~2-m-thick, normally graded conglomerate, which is clast-supported in the lower part and disorganized and matrix-supported in the upper part (insert). MPS is ~36-cm, outsized clasts are up to 1 m; Chilishtak Two section. (d) Lower Khingou Formation, Obi Khudkham section. Up to decimeter-thick, tabular, cobble-sized conglomerates are intercalated with m-thick, brick-red siltstones. Note smaller clast size compared to (a)–(c). (e) Clast-supported conglomerate with rounded to well-rounded cobbles, lower Khingou Formation, Obi Khudkham section. (F) Stacked conglomerate sheets form monotonous tabular successions with growth strata; middle Khingou Formation, Shurobod Pass section.

by pedogenic processes and bioturbation are common. At Obi Khudkham, the lithofacies of the upper Khingou Fm is comparable to the lower and middle parts of the formation. The stacked sediment packages are wedge-shaped and taper out laterally toward the east. Dip angles of the strata continue to decline upsection.

4.2.2.2. Depositional Environment

A distal alluvial plain environment in the Oligocene was replaced by a proximal mass flow depositional setting in the early Miocene. In the lower and middle Khingou Fm, stacked tabular packages of debris-flow and hyper-concentrated-flow deposits form extensive alluvial fans. Individual conglomerate beds are laterally continuous for hundreds of meters, suggesting unconstricted, sheet-like deposition on the fan surface (Bull, 1977). Repeated occurrences of fining-upward successions and transitions from debris to hyper-concentrated flows imply deposition under waning flow conditions in a proximal alluvial fan (Nemec & Steel, 1984). Coherent mudflows occur in medial alluvial fan settings. Pedogenically overprinted mudflow deposits indicate temporarily abandoned fan lobes. The Chilishtak Two and Shurobod Pass sections represent proximal to midfan positions; the Obi Khudkham section represents a midfan position. The near-absence of fine-grained lithofacies between individual alluvial fans in the lower to middle Khingou Fm indicates the coalescence of alluvial fans, forming a bajada-like, ~N-S oriented belt (present coordinates), fringing the emerging Pamir front. The continuous occurrence of subrounded clasts indicates primary rounding, suggesting storage elsewhere in the drainage basin prior to the deposition in mass-flow deposits. Broad channelized fluvial systems evolved on top of the alluvial fans in the upper Khingou Fm.

4.2.2.3. Sedimentation Rate, Stratal Pattern Architecture, and Basin Type

The ~8-Myr duration (early Miocene) and the ~1,350-m thickness of the Khingou Fm approximate an apparent sedimentation rate of ~169 m/Myr. Variable sediment thicknesses and changing lithofacies imply locally different sedimentation rates. While the strata in the lower Khingou Fm are laterally continuous, the westward thickening, eastward thinning (present coordinates), and tapering-out units indicate growth strata (Figure 7f) in the middle and upper Khingou Fm. The area-wide occurrence of coalescing alluvial fans indicates sharp facies gradients. The growth strata imply the transformation of the Tajik Basin from a foreland basin into an incipient fold-thrust belt in the early Miocene.

4.3. Synorogenic Stage II: Fold-Thrust Belt

The foreland basin was transformed into the Tajik fold-thrust belt in the middle Miocene to early Pliocene, characterized by the growth of ~N trending (present coordinates) anticlines and synclines. Based on the evolution of the depositional environment, stratal pattern architecture, sediment thickness, and transport directions of the Tavildara Fm (\leq ~15–5 Ma) and Karanak Fm (~5–4 Ma), this stage is subdivided into two sub-stages (Figures 3 and 4).

4.3.1. Substage IIa: Early Fold-Thrust Belt—Rising Morphology

4.3.1.1. Description

The middle to late Miocene Tavildara Fm (Figure 3) is ~2,300 m thick at Obi Khudkham; at Shurobod Pass, Shurobod South, Shurobod North, Daraioab Pass, and Imam Askar, only parts of the Fm are exposed (Figure 6c). The section—constructed from these exposures—is ~1,500 m thick with lithofacies variations from north to south. In the south, at Shurobod South, Shurobod Pass, Shurobod North, Daraioab Pass, and Imam Askar, clast-supported conglomerates (LFTs 4 and 6) dominate the Tavildara Fm (Figure 8a). At Shurobod Pass, the base has alternating, 5- to 10-m-thick, light-gray, clast-supported, and cobble-sized conglomerates (LFT 4) and beige-gray, horizontal-laminated to cross-bedded sandstones (LFTs 7 and 10). The average clast size is 1–8 cm (Figure 6c); clast imbrication is common. The sandy matrix is well sorted. Overlying this unit are up to 100-m-thick packages of strongly amalgamated, pebble- to cobble-sized, clast-supported conglomerates (LFTs 4 and 6). The sandy matrix of these conglomerates is well sorted, and the subrounded to well-rounded clasts are imbricated. Faint horizontal-lamination and trough cross bedding is common. Here downstream-accretion macroforms occur (Figure 9). At Shurobod South, the basal Tavildara Fm is composed of 20- to 50-m-thick, tabular packages of light-gray, clast-supported, cobble-sized conglomerate beds (LFT 4) that fine upward and occasionally grade into coarse-grained massive sandstone at the top (LFT 8). At Shurobod North, Daraioab Pass, and Imam Askar, the middle and upper Tavildara Fm is composed of 10- to 50-m-thick, amalgamated and clast-supported conglomerates (LFTs 4 and 6), comparable to the exposures at Shurobod Pass. Subrounded to well-rounded and well-sorted clasts of 3- to 10-cm average size, 10–30 cm MPS (Figure 6c), and a well-sorted sandy matrix are the characteristic features of the



Figure 8. Field examples and lithofacies (LFT; Table 2) of the Tavildara Formation. (a) Densely stacked, laterally consistent clast-supported conglomerates, Shurobod North section. (b) Clast-supported conglomerate composed of well-rounded, elongated, weakly imbricated particles, Imam Askar section. (c) Trough cross-bedded sandstone lens tapering out laterally in clast-supported conglomerate, Daraiob Pass section. (d) Upward-coarsening, debris-flow deposit containing outsized clasts of up to 2-m, Obi Khudkham section. (e) Angular unconformity at the transition from the middle to the upper Tavildara Formation.

Tavildara Fm at Shurobod Pass, Shurobod South, Shurobod North, Daraiob Pass, and Imam Askar. Clasts are densely packed, mostly elongated, and regularly imbricated. Occasionally, 20- to 50-cm-thick and 1- to 4-m-wide lenses of beige-gray, horizontal-laminated to trough cross-bedded sandstone (LFTs 7 and 10; Figures 6c and 9) are intercalated at Shurobod Pass and Daraiob Pass. Paleocurrent measurements derived from imbricated clasts at Shurobod South, Shurobod North, Daraiob Pass, and Imam Askar imply W to SW directed flow (Figure 10).

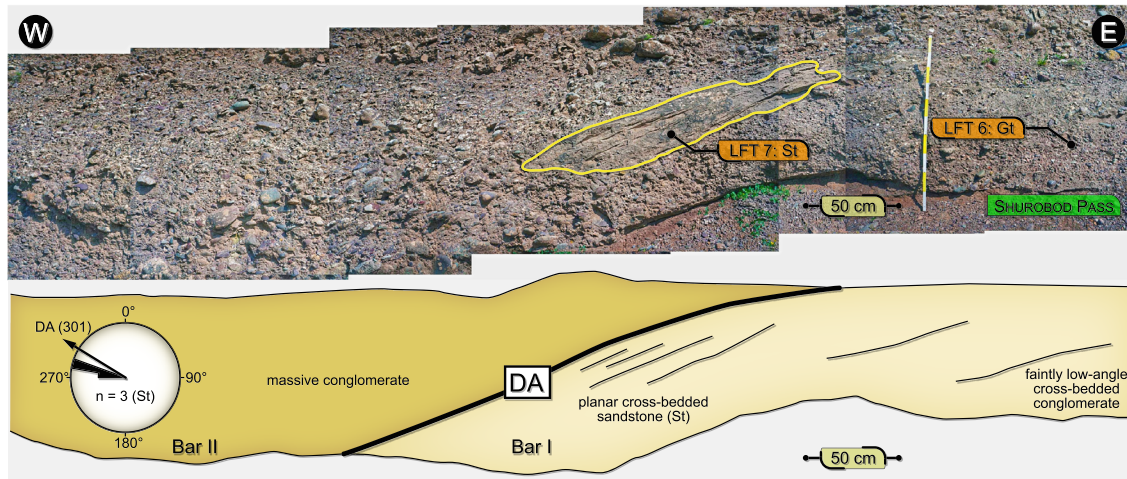


Figure 9. Downstream accretion macroform (DA) in the lower Tavildara Formation, Shurobod Pass section.

In the north, at Obi Khudkham, the Tavildara Fm resembles the underlying Khingou Fm. Stacked beds of 1- to 3-m-thick, matrix- to clast-supported conglomerates (LFTs 2 and 3) form 30- to 150-m-thick, amalgamated tabular packages. Internal stratification is typically absent. Subangular to rounded, partially elongate clasts show an average size of 6–12 cm and 20–60 cm MPS; they are supported in a reddish to red-brown, sandy to granule, moderately sorted matrix. Normal gradation is frequent and clasts occasionally form imbricated nests. Sporadically, 1- to 3-m-thick, matrix-supported, coarsening upward conglomerate beds (LFTs 1 and 2) occur with angular to subrounded, up to 200-cm-sized clasts at their top (Figure 6c). Conglomerate deposition terminated in the uppermost Tavildara Fm at Karanak Crook, where the overlying Karanak Fm consists of red-brown and gray-beige sandstones and siltstones.

4.3.1.2. Depositional Environment

In the middle Miocene, sediment gravity flows, such as debris and hyper-concentrated flows, dominated the deposition in the proximal to medial zones of large fans. In the down-fan direction, these ≤ 1 -km-wide, proximal zones transitioned into several kilometer-wide distal zones, where gravity flows and fluvial processes dominated deposition. In the distal zones, the relocation of broad and shallow, laterally unconfined channels formed the tabular conglomerate packages and prevented the construction of the thicker beds of overbank deposits (Nichols & Fisher, 2007). The sequences at Obi Khudkham indicate a proximal to medial fan position; the fluvial deposits at Shurobod South, Shurobod Pass, Shurobod North, Daraioab Pass, and Imam

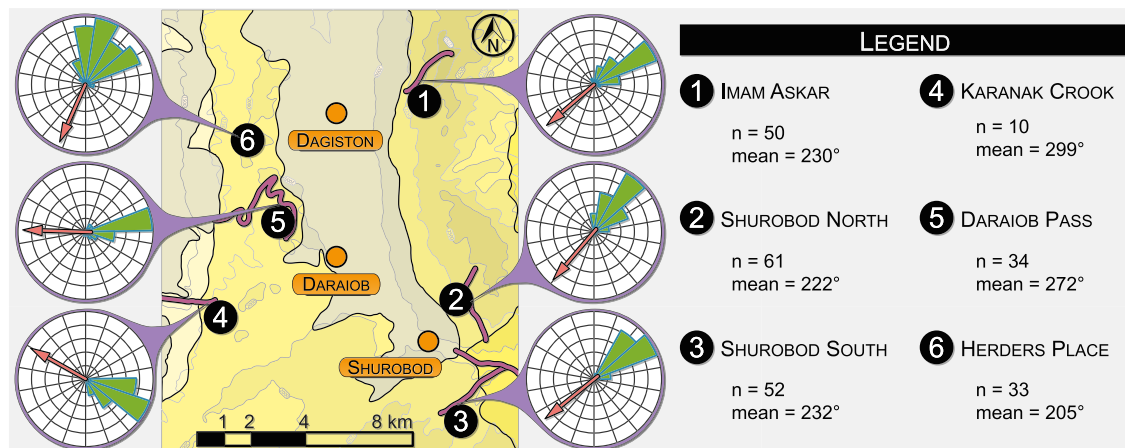


Figure 10. Paleocurrent directions derived from clast imbrication, Tavildara Formation. All orientations were corrected for structural tilt but not for vertical-axis rotations.

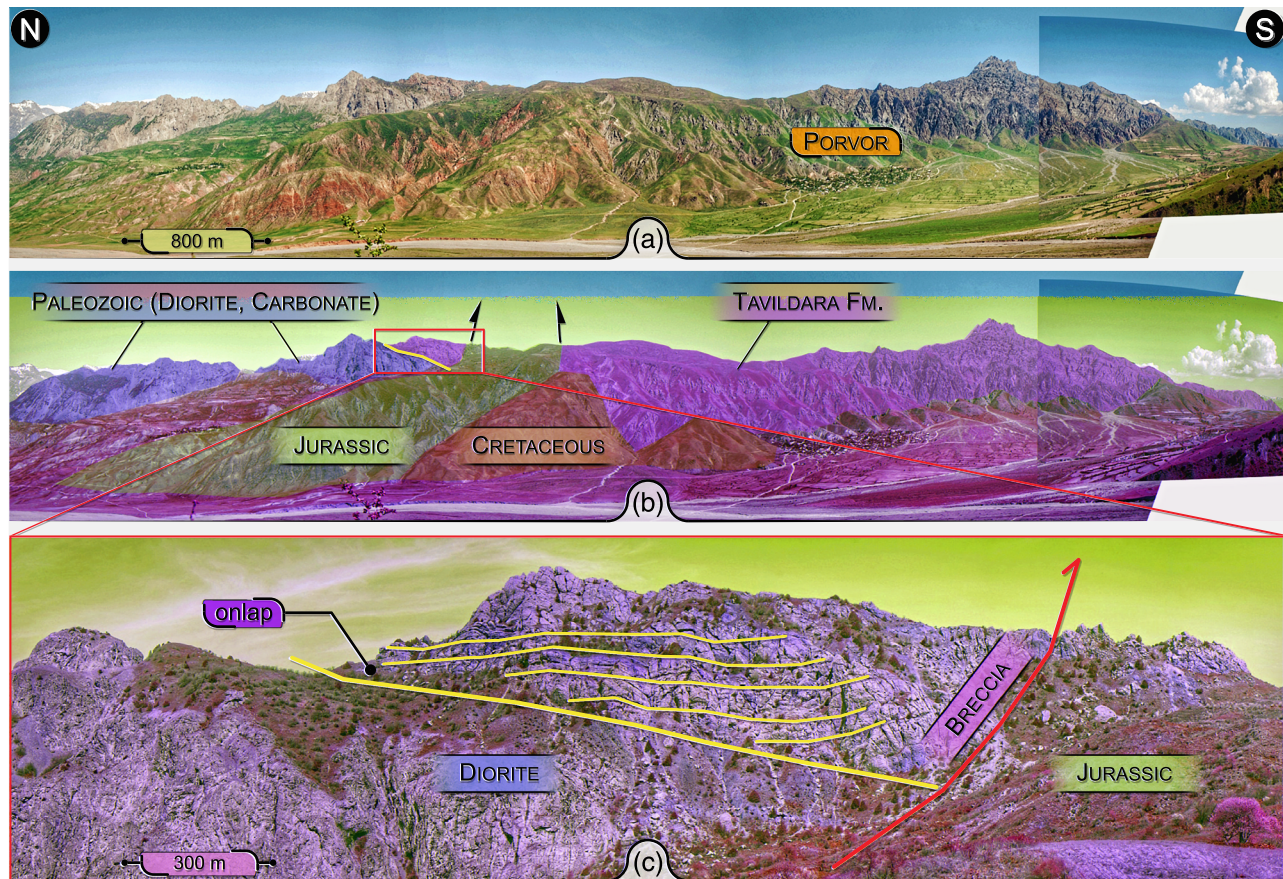


Figure 11. (a) Mountains east of the Parapanj valley near Porvor (Figure 1 for location). (b) Overlay highlights the stratigraphic assessment of the deposits. (c) Onlap of synorogenic, Miocene strata (mostly Tavildara Formation) onto Paleozoic basement rocks, suggesting the successive fill of an ~E trending paleovalley.

Askar suggest a distal fan position. Compared to the Khingou Fm, the Tavildara-Fm clasts are better rounded. The enhanced matrix sorting implies increased and more continuous discharge, resulting in enlarged fan areas. The coarse fluvial deposits occur in a > 15-km-wide belt, forming a braidplain (gravelly braided zone of Shukla et al., 2001). Mostly W to SW oriented paleocurrents imply a variable and distributed drainage network with frequent avulsion events throughout the late Miocene (Figure 10), constituting a regularly fed, laterally shifting river system that formed a fluvial mega-fan (Horton & DeCelles, 2001; Shukla et al., 2001) emanating from the Pamir. Characteristic for the fluvial mega-fan is the > 10-km lateral extent of almost indistinguishable fluvial conglomerates perpendicular to the orogenic front.

4.3.1.3. Sedimentation Rate, Stratal Pattern Architecture, and Basin Type

The ~10-Myr duration (middle to late Miocene) and the ~1,500- to 2,300-m thickness of the Tavildara Fm approximate an apparent sedimentation rate of $\geq \sim 190$ m/Myr. Sediment thickness decreases from north (Obi Khudkham) to south (Shurobod sections). Lithofacies in the north consists of matrix- to clast-supported, sediment gravity flow-dominated conglomerates, which transition to clast-supported fluid gravity flow-dominated conglomerates in the south. Growth strata occur in the north—at Obi Khudkham—throughout the Tavildara Fm; in the south—in the Shurobod area—growth strata are confined to the lower-middle Tavildara Fm. At Imam Askar, a shallow angular unconformity separates the middle from the upper Tavildara-Fm. deposits (Figure 8e). In the southeast of the study area, near the village of Porvor (37°44'N, 70°13'E; Figure 11), strata of the Tavildara Fm discordantly overlie Permian basement rocks and extend into the Pamir interior. The stratal onlap suggests the filling of an ~E trending paleo-valley. Compared to the early Miocene, the proximal parts of the fan system shifted in the middle to late Miocene from the Shurobod area in the south to Obi Khudkham in the north and toward the southeast,

into the Pamir hinterland. This indicates the formation of a basin-internal morphology in the eastern Tajik basin during initial fold-thrust belt formation.

4.3.2. Substage IIb: Fold-Thrust Belt—Reorganization of the Drainage System

4.3.2.1. Description

The red-brown to pale-brown and gray-beige sediments of the early Pliocene Karanak Fm (Figure 3) are ~1,050-m thick in the Karanak Crook section. A sharp boundary, likely a disconformity, separates the Tavildara and Karanak Fms on a regional scale; at Karanak Crook, we mapped a shallow angular unconformity. The Karanak Fm comprises meter- to decameter-thick siltstones and sandstones (LFTs 7, 10, and 12), occasionally intercalated with 1- to 4-m-thick conglomerates (LFT 6). The lower Karanak Fm has ≤60-m-thick packages of red-brown, horizontal-laminated, and pedogenic modified siltstones (LFT 12). Rootlets, subvertical bioturbation, color mottling, and carbonate nodules occur. These are intercalated with 1- to 5-m-thick pale brown to gray, trough cross-bedded, fine- to coarse-grained sandstones (LFT 7) and 1- to 4-m-thick, trough cross-bedded and clast-supported, pebble-sized conglomerates (LFT 6). The sandstones and conglomerates taper out laterally and have an erosive and scoured base, punctuated by layers of rip-up clasts. The middle Karanak Fm consists of 3- to 50-m-thick gray sandstones (LFTs 7 and 10) and 2- to 30-m-thick gray-beige siltstones (Figure 12a; LFT 12). The large- to medium-scale trough cross-bedded sandstones have an erosive and scoured base; internal cross-stratification grades upward into horizontal bedding. The sandstones form broad belts, extending laterally for several hundred meters (Figure 12b). Stacked sandstone beds form up to 100-m-thick successions. Pedogenesis has occurred in intercalated horizontal-laminated siltstones. In the Cantaloupe section, ~200-m of 0.5- to 5.0-m-thick, stacked, gray-beige, fine- to coarse-grained sandstones (LFTs 7 and 10) crop out. The bases of these beds are erosive and have cross-bedded, clast-supported, pebble-sized conglomerates (LFT 6), and trough cross-bedded pebbly sandstones. Internal cross stratification transitions upward into horizontal lamination. The sandstones contain nodules, impregnated layers of petrocalcic horizons (LFT 15), and interspersed ≤0.3-m-thick, greenish-gray silt- to mudstones (LFT 12; Figure 12c). At Karanak Crook, the upper Karanak Fm has 1- to 5-m-thick intercalations of red-brown siltstones and sandstones (LFTs 7, 10, and 12). The siltstones show mottling, calciferous cementation, and pedogenesis. Horizontal-laminated sandstones and trough cross-bedded sandstones (Figure 12d) have erosive bases and laterally variable thickness. The thickness and the abundance of sandstones decrease upsection.

4.3.2.2. Depositional Environment

The change from the upper Miocene, coarse-grained, proximal fan deposits to the lower Pliocene, fine-grained floodplain environments likely resulted from formation of a basin-internal morphology, for example, the homocline along the western Pamir front (Figure 2b). Broad and shifting fluvial channels traversed the eastern Tajik Basin, forming shallow and sandy braided river systems (Figure 12e). The change from large- to medium-scale trough cross to horizontal bedding from the base to the top of the channel deposits reflects episodes of high sediment discharge followed by waning flow conditions. The main channels trend ~N (present coordinates). Calcisols in the floodplain fines imply periods of nonsedimentation in a warm and semiarid environment. Toward the middle Pliocene, sediment load decreased and floodplains predominated.

4.3.2.3. Stratal Pattern Architecture and Basin Type

The axes of the main channels trend ~N (present coordinates) in the Karanak Fm; they roughly reflect the flow directions of the rivers due to their braided, low sinuosity character (Cain & Mountney, 2009). The change of the sediment-transport directions from broadly west directed (present coordinates) in the Tavildara Fm to broadly south directed in the Karanak Fm implies basin internal morphology able to reroute major rivers. The deposits of the Karanak Fm at Karanak Crook and Cantaloupe form an ~12-km-wide, ~N trending syncline (Figure 13). This indicates active ~E-W shortening (present coordinates) during the early Pliocene.

5. Results: Petrography and Geochemistry of the Synorogenic Strata

5.1. Sandstone Granulometry and Petrography

We analyzed thin sections from sandstones, representing the reddish and gray end-members of the Chilishtak One, Shurobod Pass, Daraiob Pass, Karanak Crook, and Cantaloupe sections (Figure 14); the red color is due to iron-oxide grain coating. The sandstones are medium- to well-sorted, immature to

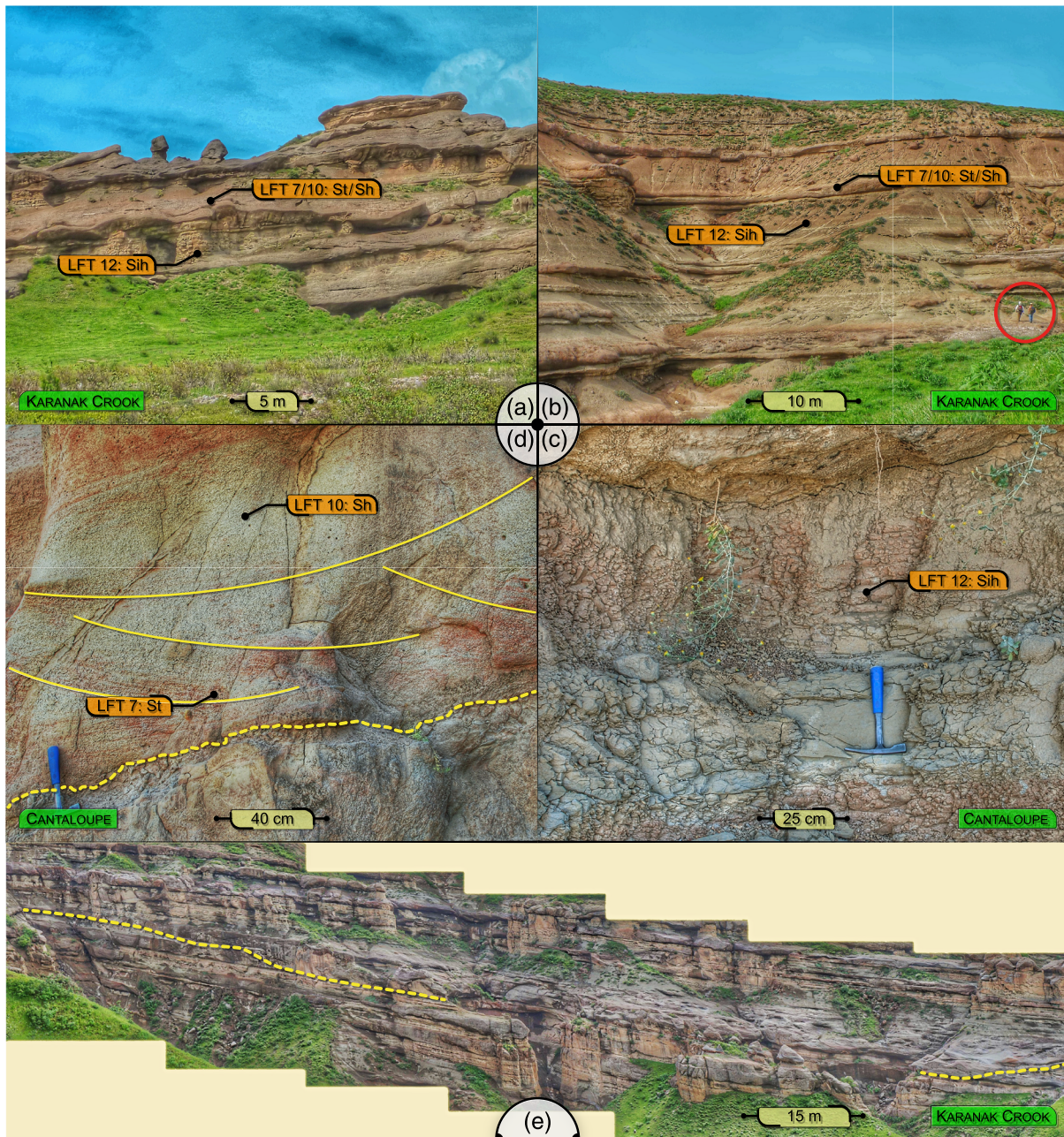


Figure 12. Field examples and lithofacies (LFT; Table 2) of the Karanak Formation. (a) Erosive, 2- to 5-m-thick, fluvial sandstone channels incised into fine-grained floodplain deposits, Karanak Crook section. (b) Thick floodplain siltstones dominating over ~1-m-thick fluvial sandstone units in the upper part of the Karanak Formation, Karanak Crook section. (c) Destratified, pedogenic siltstones with color mottling, Cantaloupe section. (d) Trough cross-bedded to horizontal-laminated fluvial sandstones, Cantaloupe section. (e) Bedforms of broad and shallow channels, Karanak Crook section.

submature, coarse- to medium-grained with angular to rounded grains; the grain size drops in the Karanak Fm.

Quartz constitutes on average 35% of the sandstones (Figure 14, QFL diagram) with monocrystalline (90% of total quartz) dominating over polycrystalline grains (10%). The majority of the former is elongate and shows undulatory extinction. Grain boundaries are straight. Polycrystalline quartz grains with less than three crystals per grain are equally abundant in the Baljuvon, Khingou, and Tavildara Fms, whereas polycrystalline quartz grains with more than three crystals dominate in the Karanak Fm. Generally, all polycrystalline grains display straight intragranular boundaries, exhibit straight extinction, and are of subequant shape.

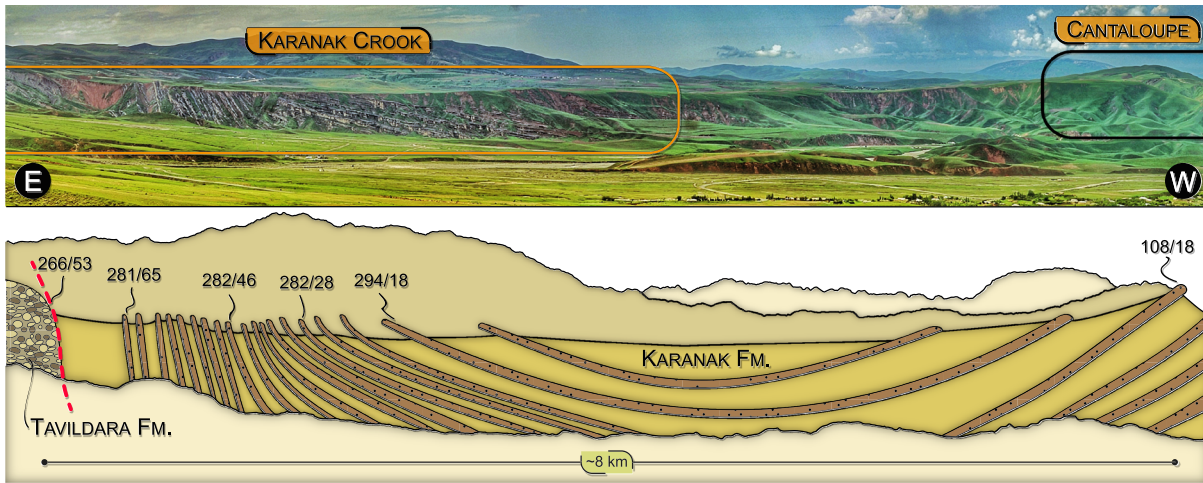


Figure 13. Cross-section, depicting the angular unconformity between the conglomeratic Tavildara and the sandy Karanak Formations and syndepositional, ~E-W shortening of the Karanak Formation along the Karanak Crook and Cantaloupe sections. See Figure 2 for location.

Feldspars constitute 10–34% of the sandstones. K-feldspars, mainly untwinned orthoclase, twinned sanidine, and subordinate microcline dominate over saussuritized plagioclase (~12% of the feldspars; Figure 14, QPK diagram). White mica occurs in the lowermost Baljuvon Fm and upper Karanak Fm. Sedimentary (Ls), meta-sedimentary (Lm), and volcanic lithics (Lv) occur in variable proportions throughout the Fms

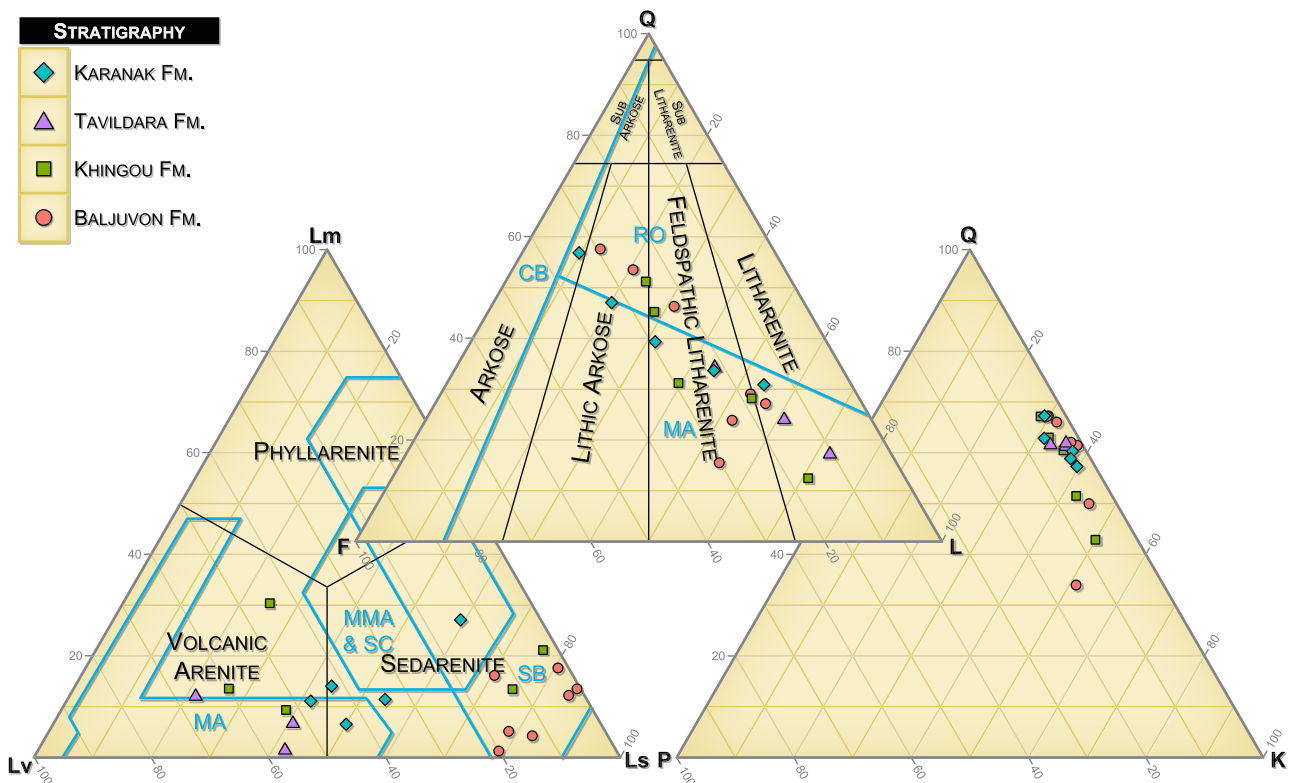


Figure 14. Sandstone composition from point counting. QFL: Arenite classification according to Folk (1974). Note the low maturity of the samples. Provenance classification after Dickinson et al. (1983). QPK: Classification displays moderate amounts of quartz and the predominance of K-feldspar over plagioclase. LmLvLs: LmLvLs-diagram with provenance fields after Ingersoll and Sucek (1979) and rock fragment classification according to Folk (1974) to further subdivide the lithic components. CB = continental block, MA = magmatic arc, MMA = mixed magmatic arc, RO = recycled orogen, SB = suture belt, SC = subduction complex.

(Figure 14, LmLvLs diagram) with sedimentary lithics being more abundant than volcanic rock fragments; meta-sedimentary lithics constitute the least abundant lithic type. Some Baljuvon-Fm sandstones show 10–15% pseudo-matrix derived from weathered lithic clasts; generally, however, such pseudo-matrix is rare. Calcite (~20%) and iron oxides are the dominant cements of the sandstones; anhydrite occurs subordinately. The modal composition of the sandstones varies from arkosic to litharenitic (Figure 14, QFL-diagram). Their low compositional maturity reflects short transport distances. The increased sorting of the conglomeratic matrix in the Tavildara Fm compared to the Khingou Fm (see section 4.2.2.1.) is not accompanied by an increase in the sandstone maturity.

5.2. Bulk-Rock Geochemistry

We analyzed 235 siltstones (LFT 12) for major oxides and 48 for trace elements. The samples are from the Baljuvon to Karanak Fms of the southern sections (Shurobod Pass, Chilishtak One, Shurobod South, Shurobod North, Daraiob Pass, Karanak Crook, and Cantaloupe) and from the Baljuvon and Khingou Fms in the north (Obi Khudkham); there are no suitable siltstones in the Tavildara Fm. Tables S1 and S2 provide the analytical data and correlations between the geochemical data.

5.2.1. Major Elements

SiO₂ contents span 36.1–69.8 wt-% with a mean of 56.1 wt-%. Al₂O₃ and CaO have means of 11.4 and 10.6 wt-%, respectively. We used Al₂O₃ to investigate the relationship between the major elements; Al₂O₃ is considered immobile during transportation, deposition, diagenesis, and weathering (e.g., Descourvieres et al., 2011; Rudnick & Gao, 2003; Taylor & McLennan, 1985). Al₂O₃ correlates positively with the major elements. Positive correlation of Al₂O₃ with Fe₂O₃, MgO, K₂O, and TiO₂ suggests a common source, likely the detrital sediment fraction, that is, feldspars and clay minerals (Das et al., 2006). In contrast, CaO and MnO do not correlate with Al₂O₃, indicating their derivation from secondary mineral phases, likely pedogenic precipitates.

We compared the ratios of several major elements for chemical classification and discrimination between mature and immature rocks: Al₂O₃/SiO₂ compares the abundance of quartz with that of clay minerals and feldspars (Potter, 1978), and Fe₂O₃/K₂O distinguishes lithic fragments from arkoses (Herron, 1988). The Baljuvon-Fm samples comprise litharenites, wackes, and shales. The Khingou-, Tavildara-, and Karanak-Fm samples comprise wackes and shales (Figure 15a). The low maturity of the fine-grained, suspension-load lithofacies, obtained from bulk rock geochemistry, corresponds to that of the bed-load sandstone lithofacies, obtained from optical microscopy (see section 5.1.). There is no significant compositional trend from older to younger strata.

5.2.2. Trace Elements

5.2.2.1. Large Ion Lithophile Elements: Rb, Cs, Ba, and Sr

Rb abundances are slightly depleted but similar to the upper continental crust (UCC; Rudnick & Gao, 2003; Hu & Gao, 2008). Sr and Ba are significantly depleted ($0.66 \times$ UCC and $0.69 \times$ UCC, respectively), and Cs is enriched ($1.34 \times$ UCC; Figure 15b). Except for Sr and Ba, the large ion lithophile elements and the trace elements Rb and Cs correlate positively ($r = 0.72$ and $r = 0.65$) with Al₂O₃. Therefore, phyllosilicates control their abundances (e.g., McLennan et al., 1993). Rb and Th are strongly correlated ($r = 0.90$), implying similar geochemical behavior, and both are strongly correlated with K₂O ($r = 0.95$ and $r = 0.88$), suggesting derivation from K-bearing clay minerals. This indicates that Rb and Cs originate from the detrital fraction, whereas Ba and Sr likely are from the pedogenic precipitates.

5.2.2.2. High Field Strength Elements (HFSE): Th, U, Zr, Hf, Y, and Nb

The high field strength elements reflect the chemical composition of the source-area rocks due to their immobility (Taylor & McLennan, 1985). Additionally, they are enriched in felsic rocks due to their preferred partitioning into melts during crystallization (Feng & Kerrich, 1990). In comparison with the UCC (Figure 15b), Zr, Hf, and Nb are slightly depleted ($0.92 \times$ UCC, $0.88 \times$ UCC, and $0.91 \times$ UCC), while Y is slightly enriched ($1.07 \times$ UCC). Due to their similar chemical properties, Zr and Hf behave geochemically coherent ($r = 0.96$), as do Th and U ($r = 0.64$). The Zr/Hf ratios of 32.77–42.75 are almost identical to that of zircon (Murali et al., 1983), suggesting that zircon controls the Zr and Hf content of the detrital fraction. In contrast, Zr does not correlate with the heavy rare earth elements. Th strongly correlates with a number of other elements (Table S2), especially the rare earth element (REE), such as Yb and Ho ($r = 0.91$ and $r = 0.89$),

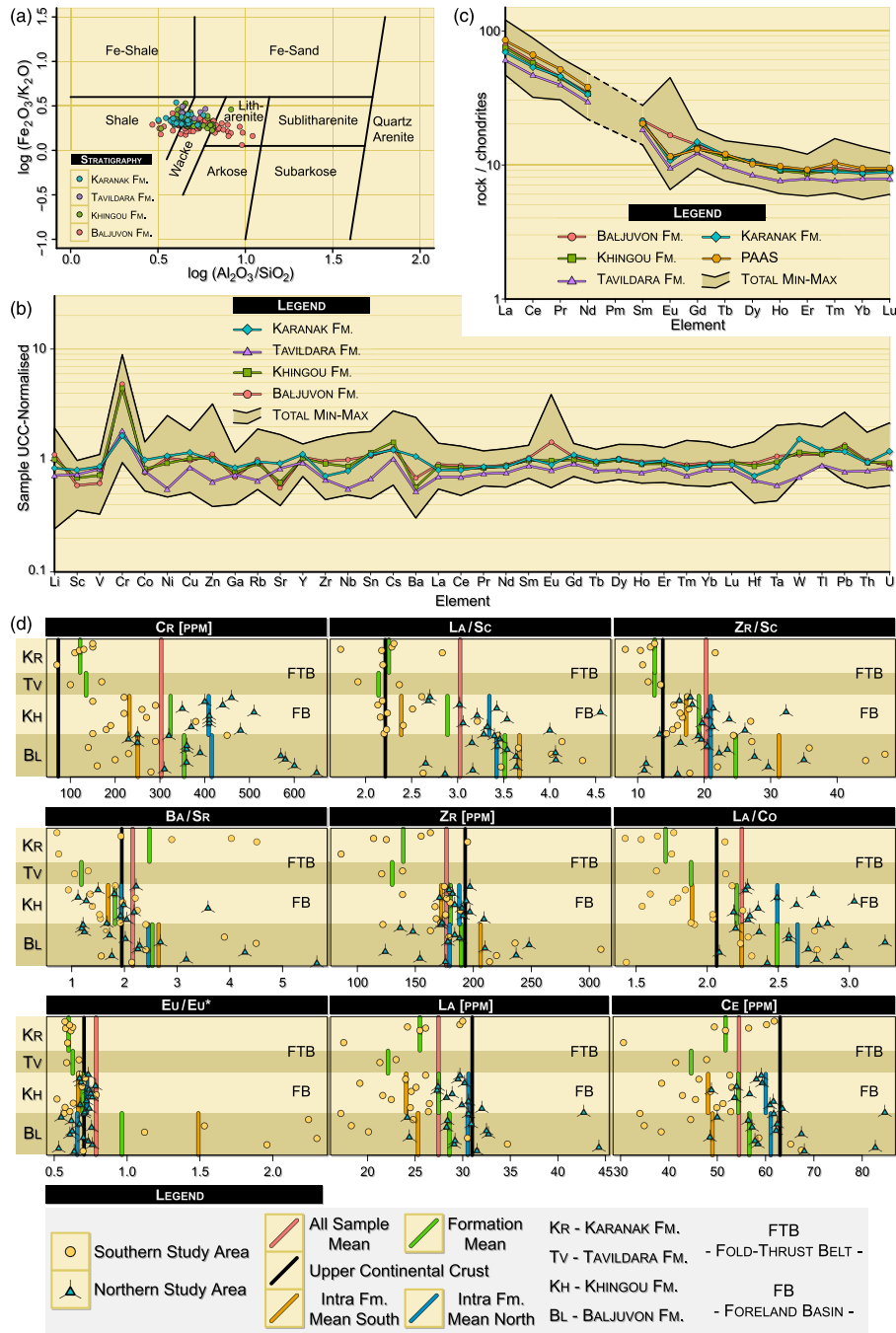


Figure 15. Geochemistry of the synorogenic strata. (a) Log ($\text{Fe}_2\text{O}_3/\text{K}_2\text{O}$) vs. log ($\text{Al}_2\text{O}_3/\text{SiO}_2$) plot for geochemical classification of terrigenous sands and shales (Herron, 1988) of the siltstone samples. Note the overall low maturity of the siltstones. (b) Spider diagram of trace elements (formation means) normalized against the upper continental crust (UCC; values of Rudnick & Gao, 2003; Hu & Gao, 2008). Trace elements are depleted in the Tavildara Formation in comparison to those of the Baljuvon, Khingou, and Karanak Formations. (c) Spider diagram of rare-earth elements (Formation means) normalized against the C1 chondrites (normalizing factors according to Taylor & McLennan, 1985). Post-Archean average Australian Shale (PAAS; values according to Nance & Taylor, 1976) plotted for reference. Depletion of rare-earth elements in the Tavildara Formation compared to those in the Baljuvon, Khingou, and Karanak Formations; positive Eu anomaly in the Baljuvon Formation. (d) Scatterplots of selected trace elements and trace-element ratios, displaying variable depletion or enrichment within the different stratigraphic units in relation to upper continental crust concentrations. Samples of the southern study area are from the Baljuvon (Chilishtak One and Shurobod Pass sections), Khingou (Shurobod Pass section), Tavildara (Shurobod South and Shurobod North sections), and Karanak Formations (Karanak Crook section); samples of the northern study area are from the Baljuvon and Khingou Formations (Obi Khudkham section). All sample mean = the average of all synorogenic Formations; formation mean = the average for individual Formations; Intra Fm. Mean South = average of Baljuvon and Khingou Formations at Chilishtak One and Shurobod sections; Intra Fm. Mean North = average of Baljuvon and Khingou Formations at Obi Khudkham section. FB (foreland basin) and FTB (fold-thrust belt) denote the stages of synorogenic basin evolution.

which implies control by clay minerals and/or associated phases (e.g., oxides, hydroxides, and silicates; Mukherjee, 2013).

5.2.2.3. Transition Trace Elements: Cr, Co, Ni, V, Sc, and Cu

Most transition trace elements abundances correspond to those of the UCC, for example, Ni and Cu ($0.99 \times \text{UCC}$ and $1.03 \times \text{UCC}$; Figure 15b). Co, V, and Sc are depleted ($0.84 \times \text{UCC}$, $0.72 \times \text{UCC}$, and $0.68 \times \text{UCC}$), and Cr is enriched ($4.17 \times \text{UCC}$). All transition trace elements except Cr are correlated with Al_2O_3 ; Sc and V most significantly ($r = 0.92$; $r = 0.90$). Thus, these elements are associated with the detrital fraction (Feng & Kerrich, 1990).

5.2.2.4. Rare Earth Elements (REE)

The REE abundances correspond to those of the UCC. Although the REE are considered to be incorporated into detrital minerals like zircon and monazite (McLennan, 1989), positive correlations between ΣREE and Al_2O_3 , MgO, TiO_2 , K_2O , and Fe_2O_3 ($r = 0.70, 0.60, 0.84, 0.82,$ and 0.71) suggest that phyllosilicates and probably Fe- and Ti-bearing oxides are also important in hosting the REE. In contrast, the REE exhibit a low correlation with Zr ($r = 0.30$; Table S2), implying that the heavy rare earth element fractionation is not controlled by the occurrence of zircon.

5.2.2.5. Interformation and Intraformational Variations

UCC- or chondrite-normalized spider diagrams (Figures 15b and 15c) show similar element concentrations for the Baljuvon, Khingou, and Karanak Fms. In the Tavildara Fm, the concentrations for most of the elements are depleted. Only a few trace elements are enriched in comparison with the UCC. A positive Eu anomaly occurs in some samples. To highlight the compositional differences between the formations and the northern and southern sections, Figure 15d shows single trace element and element-ratio plots. The concentrations of some elements (Cr, Zr, La, and Ce) and the ratios of La/Sc, Th/Sc, Zr/Sc, and La/Co are indicators of sediment-source composition (e.g., Taylor & McLennan, 1985). These show shifts within individual Formations and over time. The Baljuvon and Khingou Fms at Obi Khudkham have mean Cr values of 415 and 408 ppm, whereas at Shurobod Pass, they are 250 and 231 ppm, and thus are slightly depleted compared to the Formations in the northern study area. The same applies for La, Ce, Rb, Li, Zn, Ta, Ni, and La/Co, Cr/V, and Cr/Th (Figure 15d). As the Tavildara and Karanak Fms do not crop out at Obi Khudkham, it remains open if the intraformational variations of those elements and element ratios are a general feature. At Shurobod Pass, the Cr, Zr, La, Ce, Hf, and Li concentrations and the La/Sc, Th/Sc, Zr/Sc, La/Co, Cr/V, and Cr/Th ratios show lower values in the Tavildara and Karanak Fms than in the underlying Baljuvon and Khingou Fms. The Eu/Eu* ratio attains lower values already at the boundary between the Baljuvon and Khingou Fms. The majority of elements and element ratios signal a change in source composition in the Tavildara Fm, coinciding with the transformation of the Tajik basin from a foreland basin into a fold-thrust belt. The Ba/Sr and Rb/Sr ratios are robust weathering indicators, except for intense weathering, where significant loss of the large ion lithophile elements can occur (e.g., Gallet et al., 1996; Muhs et al., 2001). Ba/Sr shows the highest mean values in the samples from the Baljuvon and Karanak Fms, while the ratio is significantly lower in the Khingou and Tavildara Fms. This suggests stronger chemical weathering in the Baljuvon and Karanak Fms, probably due to longer surface exposure of the sediments compared to the Khingou and Tavildara Fms.

6. Discussion

Here, we return to the goals of this study. First, we aimed to use stratigraphic and sedimentologic observations from the Cretaceous-Pliocene strata along the eastern margin of the Tajik basin to describe the depositional environment, drainage evolution, and stages of basin formation. Then, we intended to utilize sediment petrography and geochemistry to detect vertical, that is, time-dependent changes in the stratigraphic column, and relate those to source-area changes in the hinterland. Having defined the stages of the evolution of the eastern Tajik basin in the Shurobod area, we next aimed to integrate our results with those ~100 km farther north, in the Tavildara-Sary Ob region at the northeastern margin of the Tajik basin (Figure 1c; Klocke et al., 2017). Finally, we aimed to link the phased evolution of the Tajik basin with the major stages of the tectonic evolution of the Pamir hinterland, reviewed in section 1. Establishing such interpretative links, we are faced with the major problem that has hampered all studies of the synorogenic deposits of the Tajik basin: the imprecise age assignment of its Formations, in particular the Baljuvon to Karanak Fms. Recent progress in age calibration of the preorogenic (Bosboom et al., 2015; Kaya et al., 2019) and

synorogenic deposits (Abdulhameed et al., 2020; Chapman et al., 2019) contributed to a more reliable timing of the Formation boundaries (Figures 3 and 4). However, as precise depositional ages are still lacking for the synorogenic Formations—the detrital ages presented by Chapman et al. (2019) and Abdulhameed et al. (2020) are maximum depositional ages—our correlations remain preliminary. In the future, better time resolution may lead to a vertical age shift of the Formation boundaries by a few Myr, and/or, these boundaries will turn out to be regionally asynchronous. Currently, our solution is to correlate only the most notable changes in the sedimentary and tectonic evolutions.

6.1. Basin Evolution

6.1.1. Preorogenic Stage

Our study of the Shurobod area at the eastern margin of the Tajik basin corroborates earlier work throughout Central Asia (see section 3.), which showed that an alternating shallow marine to coastal environment prevailed during the Cretaceous and Paleogene, predating the rise of the hinterland. During this time, an epi-continental sag basin, characterized by low sedimentation rates of ~ 20 m/Myr (see section 4.1.) and shallow facies gradients, resulting in a layer-cake architecture, prevailed in the present-day eastern Tajik basin. The Tajik basin had marine incursions in the Late Cretaceous, late Paleocene to early Eocene, middle Eocene, and late Eocene, caused by the eastward transgressions of the Turan Sea into the Tarim basin (Bosboom et al., 2011, 2013, 2015; Carrapa et al., 2015; Kaya et al., 2019; Sun & Jiang, 2013). In the Shurobod area, the final retreat of the Turan Sea resulted in the formation of a coastal environment and an extended alluvial plain. This is expressed by widespread red beds and the absence of marine deposits in strata younger than the late Eocene Isfara-Hanabad Fm (~ 37 Ma; Kaya et al., 2019). Carrapa et al. (2015) inferred that the main phase of regression occurred at ~ 39 Ma, but as noted by Bosboom et al. (2015), this age corresponds to the regression at the top Turkestan Fm. Furthermore, Dzhililov et al. (1982) documented the occurrence of marine bivalves and snails in the Tajik basin well into the late Eocene (Kushan and Sanglak horizons, which correlate with the Isfara-Hanabad and Sumsar Fms; Figure 3). In fact, they documented oysters and stromatolites in the Hissarak member of the basal Baljuvon Fm (early Oligocene, base at ~ 34 Ma), which occurs west of the Vakhsh river (at about the position of the Vakhsh syncline in Figure 1c) and in the northern Tajik basin. The ultimate change to fully continental sedimentation thus likely occurred—in accordance with Bosboom et al. (2015)—as late as ≤ 34 Ma in the northwestern Tajik basin, coeval with the global sea level drop (Eocene-Oligocene transition).

6.1.2. Synorogenic Stage I

Beginning with the Baljuvon Fm—during the early to late Oligocene (~ 34 – 23 Ma)—a continental foreland basin formed in what is today the eastern Tajik basin. Apparent sedimentation rates increased to ~ 86 m/Myr (see section 4.2.1.). After a prolonged phase of floodplain sedimentation with only distal fluvial conglomerates (Shurisay Member, early Oligocene), the sudden basinward progradation of proximal alluvial sediments marked a major change of the depositional environment, represented by the Kamolin Member of the Baljuvon Fm; the base of the member is now dated at $\leq \sim 29$ Ma (Chapman et al., 2019). The occurrence of isolated, fan-like alluvial bodies dominated by conglomerates, representing stacked debris and hyper-concentrated flows, records the first major pulse of erosion of an elevated topography in the hinterland. Based on our paleocurrent data, these sediments were derived from sources in the east (present coordinates), that is, the Pamir. Variations in sediment thickness and laterally changing lithofacies resulted in the development of a moderate basin morphology (Figure 16a). In the early Miocene, the foreland basin was fully developed; apparent sedimentation rates sharply increased to ~ 169 m/Myr with the deposition of proximal alluvial fan deposits of the Khingou Fm, beginning at $\leq \sim 23$ Ma (see section 4.2.2.). This indicates high exhumation rates in the hinterland at that time. Coalescing alluvial fans, containing boulder-sized clasts, formed an extended bajada that fringed the western Pamir (present coordinates; Figure 16b).

6.1.3. Synorogenic Stage II

The first growth strata in the middle Khingou Fm provide sedimentologic evidence for the onset of the transition of the foreland basin into a fold-thrust belt. In the Tavildara Fm. ($\leq \sim 15$ – 5 Ma), high apparent sedimentation rates of ≥ 190 m/Myr (see section 4.3.1.) and continued development of westward thickening growth strata indicate the development of distinct and proximal hinterland topography, probably a precursor of today's frontal homocline in the eastern Tajik basin. The increased roundness of the conglomerate clasts and the better sorting of the matrix in the Tavildara Fm compared to the Khingou Fm indicate an

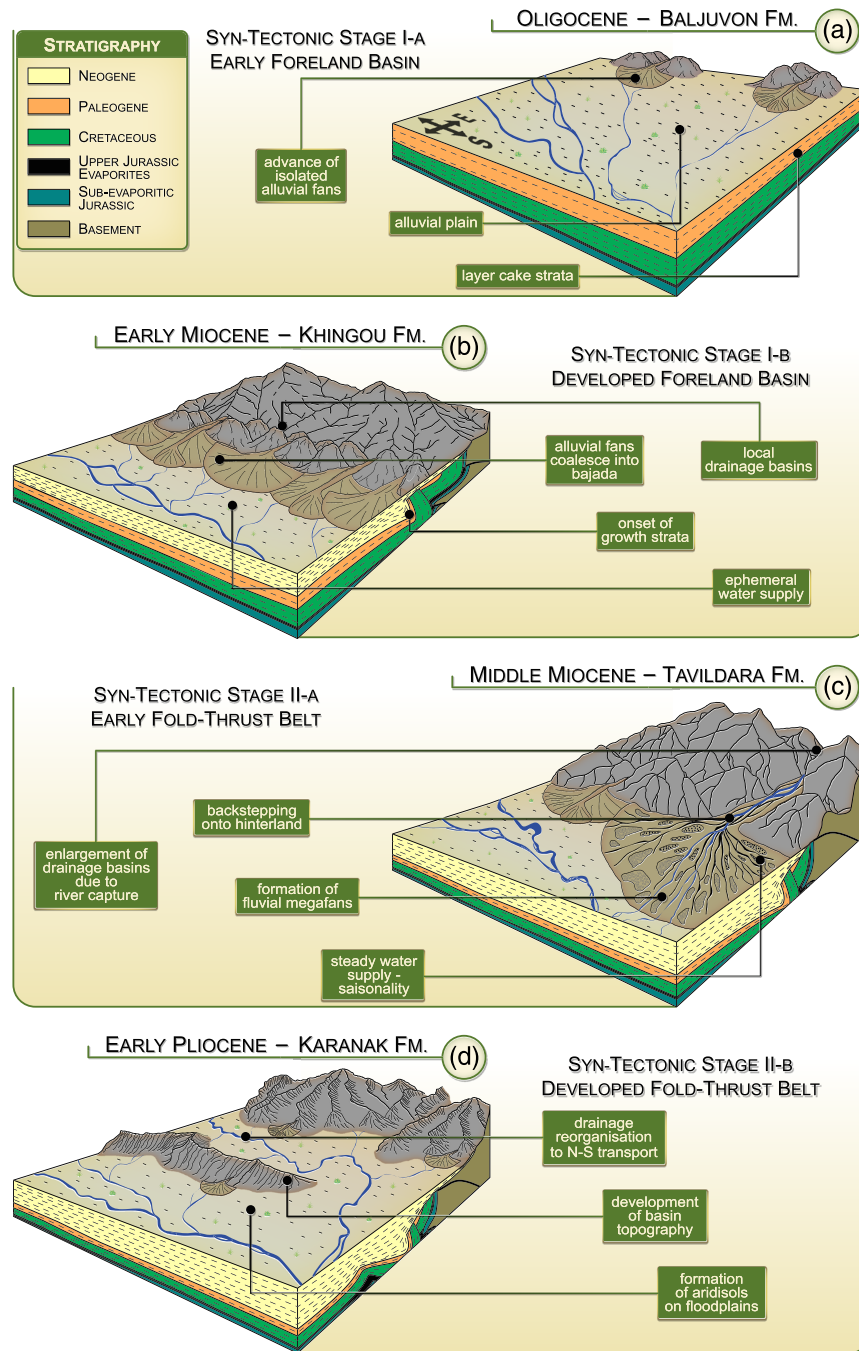


Figure 16. Reconstruction of the depositional environment and synorogenic basin evolution of the eastern Tajik basin from Oligocene to Pliocene. (a) Development and advance of isolated alluvial fans on a stable alluvial plain, evacuating sediment from the initial exhumation of the distant Pamir hinterland, transform the Tajik basin into a foreland basin. The alluvial plains are traversed by minor fluvial channels and dominated by floodplain fines. The preorogenic sediments are characterized by shallow facies gradients resulting in a layer-cake architecture, whereas locally different sedimentation rates of the early synorogenic strata indicate the development of a moderate morphology. (b) Growing alluvial fans evacuate progressively increasing sediment volumes from local hinterland drainage basins into the Tajik basin, resulting in sharply increasing facies gradients and development of morphology. High exhumation rates and evenly spaced drainage outlets along the Pamir front led to the coalescence of individual alluvial fans into a vast interconnected bajada. In the middle-late Miocene, westward thickening growth strata indicate the onset of basin inversion and the transformation of the Tajik basin from a foreland basin into the Tajik fold-thrust belt. (c) Upstream migrating incision and river capture resulted in the enlargement of the hinterland drainage basins, which along with increased water supply led to the formation of a fluvial mega-fan. High sedimentation rates and emerging intra-basin morphology filled the available accommodation space and led to back-stepping of sedimentation onto the hinterland. (d) Continuous growth of the fold-thrust belt with ridges parallel to the mountain front resulted in a major reorganization of the drainage system from transverse to longitudinal sediment transport. Main sediment evacuation was relocated to the northeastern Tajik basin, leading to the formation of extended floodplains traversed by broad and shallow braided channels of low sinuosity.

increase in water supply and perennial discharge in the former. This change from a sediment-gravity flow dominated to a fluid-gravity flow-dominated depositional environment resulted in the formation of a fluvial mega-fan in the study area (Figure 16c). Continued shortening resulted in angular unconformities (i.e., middle/upper Tavildara Fm, Imam Askar section), erosion of synorogenic strata, and increased basin morphology. The continued growth of ~N trending folds (present coordinates) in the Tajik basin blocked transversal sediment transport. The accommodation space at the eastern Tajik basin margin became overfilled, triggering the back-stepping of the basin into the hinterland in the middle Miocene. This is proven by growth strata that discordantly overlap the eroded basement of the Pamir (Figure 11). The waning and vanishing of the growth strata in the upper Tavildara Fm (~7 Ma) and the deposition of the fine-grained floodplain sediments of the Karanak Fm (~5–4 Ma) may mark the temporary cessation of shortening at the eastern margin of the Tajik basin or its relocation, causing a shift to more distal basin facies in the Shurobod area. Major sediment evacuation from the exhuming Pamir may have shifted northward (present coordinates) along the western Pamir flank in the Pliocene (Klocke et al., 2017). Our paleocurrent data mark this reorganization of the drainage system from lateral (E-W) to longitudinal (N-S) sediment transport in the eastern Tajik basin (see section 4.3.2., Figure 16d). The progressively declining dip angles of the strata in the Karanak Fm toward the center of the Kulyab syncline (Figure 11) indicate the resumption/intensification of shortening along the eastern basin margin in the Pliocene.

6.2. Drainage-Network Evolution and Provenance

The size, spacing, and character of the drainage network along a mountain front reflect the amount of sediment evacuated from the hinterland, the amount of water discharge depends—given a relatively stable climate—on the size of catchments, and the extent of orogenic exhumation through variations in the local base level of the fluvial systems (e.g., Beaumont et al., 1992; Castellort & Simpson, 2006; Frostick & Jones, 2002). Our sections along the eastern Tajik basin record the transformation of the drainage systems from an early continental foreland basin into a fold-thrust belt adjacent to the western front of the Pamir.

The extensive Oligocene (~34–23 Ma) alluvial plains mark the change from a marine-influenced depositional environment to an exclusively continental depositional environment with a rising hinterland. In the absence of large antecedent drainages, incipient uplift results in the development of small drainage networks with outlets spaced several kilometers apart along the emerging orogenic front (e.g., Beaumont et al., 1992). As numerous small streams transfer eroded material away from the emerging hinterland, isolated small-scale alluvial fans flank the mountain front (Figure 16a). These drainage areas are mostly restricted to the leading structures of the orogen (Horton & DeCelles, 2001). The growth of individual catchments results in the incorporation of additional watersheds by river capture (Koons, 1995). This creates fewer but better developed and more widely spaced drainage networks competing for catchment area. The evolving drainage networks succeed in the evacuation of the increased sediment supply from the rising frontal ranges.

The outward growth of the Pamir salient likely produced considerable shortening along the deformation front, the eastern Tajik basin (Chapman et al., 2017; see Figure 1e and details about the structural geometries and amount of shortening in Gagala et al., 2020). This promoted the incisions of small streams, headwater migration, and thus capture of upstream drainage networks; consequently, a row of closely spaced outlets replaced the established gorges along the basin margin, feeding an extending bajada (Khingou Fm, \leq ~23–15 Ma; Figure 16b) at the mountain front (cf. Clevis et al., 2003). Catchment cannibalism ultimately favored the formation of large drainage systems; fewer outlets channelized the sediment flow along the orogen front with larger drainages that reach farther into the hinterland. Large fluvial distributary systems developed at the outlets along the orogenic front during this stage (Tavildara Fm, \leq ~15–5 Ma; Figure 16c). High sediment flux filled the available accommodation space. Activation of the Tajik fold-thrust belt led to the distribution of shortening across the rising thrust-cored folds of the Afghan-Tajik depression during the middle-late Miocene (~12 Ma; Abdulhameed et al., 2020; Gagala et al., 2020). At this stage, shortening had established an intrabasinal morphology parallel to the Pamir front. This likely restricted the accommodation space and blocked further transversal sediment transport. Thus, sediment accumulation was forced to step back eastward onto the frontal homocline, establishing a floodplain environment traversed by axial rivers (Karanak Fm, ~5–4 Ma; Figure 16d) in the eastern Tajik basin. As the main sediment locus from the hinterland into the basin shifted northward (present coordinates; cf. Klocke et al., 2017), the

drainage network in the eastern Tajik basin reorganized from transverse to longitudinal to the orogenic front.

The petrography of the sandstones and siltstones reveals strong similarities between the different synorogenic Formations. Lithic arkoses and litharenites dominate the sandstones; litharenites, wackes, and shales compose the siltstones. This implies little fractionation across the grain-size spectra, pointing to a dominance of physical weathering. The immaturity of the sandstones implies little diagenetic overprint; diagenesis in sandstones intensifies the breakdown of labile grains into pseudomatrix (Dickinson, 1970) and thus increases the mineralogical maturity (Helmold, 1985).

The trace-element composition of the siltstones reflects changing sediment sources. Strong intraformational differences in the abundance of Cr, Mo, Pb, and Eu, in particular in the Baljuvon Fm but also in the Khingou Fm, occur between the northern section (Obi Khudkham) and the southern sections (Shurobod, Chilishtak One, and Chilishtak Two). This implies the presence of small and localized drainage basins, at least in the Baljuvon Fm. Intraformational differences between Cr, Mo, Pb, and Eu decrease upsection into the Tavildara Fm, reflecting better mixing and averaging of locally enriched elements in increasingly larger drainage basins. In addition, mobile elements such as Sr, Sc, V, and Cr approach values of the UCC with decreasing stratigraphic age, that is, the Oligocene Baljuvon Fm, diverge most from the average UCC composition, the Khingou Fm less, and the Tavildara Fm has UCC composition. This indicates increased mixing during transport and less dispersal due to depositional fractionation over time, thus larger drainage systems.

Hydraulic fractionation enriches the REEs in the fine-grained clastic sediments. Thus, the decrease in REE abundance from the Baljuvon Fm to the Tavildara Fm and their increase in the Karanak Fm mirrors the changes in the sedimentary environment: increasingly proximal from the Baljuvon Fm to the Tavildara Fm, and more distal in the Karanak Fm. Protracted fractionation processes in a distal alluvial plain—the Baljuvon Fm—changed to depletion in an increasingly proximal clastic environment with less weathering—the Tavildara Fm. REEs in the Tavildara Fm are preferentially tied to the coarser grain sizes, whereas in the Karanak Fm, the REE content indicates enhanced grain fragmentation and incorporation of the REE into the finer grain-size classes.

6.3. Tectonic Framework

How is the Tajik-basin evolution and its provenance record tied to Pamir tectonics? Petrochronology recorded the synchronous onset of crustal thickening across the entire South and Central Pamir—and likely the Karakorum and Hindu Kush south of it—at $\geq \sim 37$ Ma (section 1; Smit et al., 2014; Hacker et al., 2017). The onset of crustal thickening was contemporaneous with a localized pulse of magmatism in the Central Pamir at 42–36 Ma (Chapman et al., 2018; Hacker et al., 2017). In the Shurobod area, the final retreat of the Turan Sea is marked by the formation of an extended alluvial plain, indicated by the widespread red beds that are younger than the late Eocene Isfara-Hanabad Fm (top of formation at ~ 37 Ma). The onset of foreland-basin formation, in particular at its eastern margin, may be a few Myr earlier than the ultimate basin-wide establishment of fully continental sedimentation at ≤ 34 Ma (Hissarak Member) in the entire Tajik basin, coeval with the global sea level drop (section 6.1.1). We therefore speculate that the formation of the extended alluvial plain in the eastern Tajik basin is consistent with the establishment of a foreland-basin as a result of the onset of crustal thickening in the distant Pamir hinterland.

We interpreted the occurrence of isolated channelized conglomerates in the Shurisay Member followed by fan-like alluvial bodies dominated by conglomerates in the Kamolin Member to mark a major change of the depositional environment. The deposition of conglomerates and increasing apparent sedimentation rates from ~ 20 m/Myr (Paleogene) to ~ 86 m/Myr (Oligocene) indicate that the foreland basin was established. We suggest that the alluvial fans constituting the Baljuvon Fm (~ 34 – 23 Ma) represent the foreland response to crustal thickening across the entire South and Central Pamir since $\geq \sim 37$ Ma, in particular the most rapid phase of shortening and thickening at ~ 27 – 20 Ma (Figure 4; Hacker et al., 2017).

Carrapa et al. (2015) suggested that the overall stratigraphic record of the Tajik basin and the southwestern Tian Shan—together with the northwestward younging trend of the Turan-Sea regression—point to the

establishment of a foreland-basin setting at ~40 Ma. As shown by Bosboom et al. (2015) and Kaya et al. (2019), the ultimate incursion (top at ~39 Ma) of Carrapa et al. (2015) does in fact correspond to the penultimate incursion (Turkestan Fm) of the Turan Sea into the eastern Tajik basin (Figure 3). Fixing the beginning of the foreland basin stage at ~40 Ma would thus include the Rishtan to Sumsar Fms into this stage. This appears unlikely considering the fine-grained terrestrial deposits of the Rishtan and Sumsar Fms and the apparent sedimentation rate of ~20 m/Myr for the whole succession. Chapman et al. (2019) dated the foreland-basin stage back to the Early Cretaceous based on the eastward thickening of the Lower Cretaceous succession from ~600 m in the western Tian Shan to ~1.5 km along the Pamir front. Based on the ~45 Ma duration of the Early Cretaceous subsystem, the resulting maximum sedimentation rates would range from ~13 m/Myr in the western Tian Shan to ~33 m/Myr along the Pamir front. These rates compare well to the herein approximated rate of ~20 m/Myr for the Paleogene preorogenic stage but are far below the rates estimated for the synorogenic stages Ia and Ib (~86–190 m/Myr). As we focus herein on the Cenozoic evolution of the Pamir-Tian Shan orogenic system, we classify the Lower Cretaceous succession as the preorogenic stage.

The main episode of proximal, synorogenic sediment accumulation in the Tajik basin is recorded by the coalescence of proximal alluvial fans in the Khingou Fm (\leq ~23–15 Ma). These fans formed an extended bajada, indicative of the proximity to the hinterland. We interpret this major change from distal to proximal deposition as the response to the relocation of the deformation front from the Central Pamir to the North Pamir during the extensional collapse of the Central Pamir (~23–15 Ma, with decreasing rates until cessation at ~12 Ma; section 1; Rutte, Ratschbacher, Schneider, et al., 2017; Rutte, Ratschbacher, Khan, et al., 2017). This new deformation front in the North Pamir may have induced the change from the floodplain/distal alluvial fan stage in the upper part of the Baljuvon Fm to the proximal deposits in the Khingou Fm. Moreover, the largest outsized clasts, recorded in the lower Khingou Fm (~23–20 Ma), coincide with peak erosion at ~23–20 Ma in the Central and South Pamir as reported by Hacker et al. (2017) and Rutte, Ratschbacher, Khan, et al. (2017; Figure 4).

The appearance of growth strata in the middle Khingou Fm provides sedimentologic evidence for the onset of the transition of the foreland basin into a fold-thrust belt in the Shurobod area. The Tavildara Fm (\leq ~15–5 Ma) contains the most spectacular growth strata of the Tajik basin, thus signaling the major phase of fold-thrust belt formation (Figure 4). The progressive approach and ultimate onset of indentation of the Indian cratonic lithosphere into the Tajik-Tarim lithosphere underneath the Pamir and the onset of the rollback of the Tajik-basin lithosphere at ~12–11 Ma likely initiated the Tajik fold-thrust belt formation (section 1, Kufner et al., 2016, 2018; Schurr et al., 2014). The age of the sedimentologically derived major phase of fold-thrust belt formation in the eastern Tajik basin roughly corresponds to the thermochronologically determined onset of shortening in the entire fold-thrust belt at ~12 Ma (Abdulhameed et al., 2020). It also is contemporaneous with the transfer of the southwestern Tian Shan into a dextral transpressive deformation belt (section 1; Käßner et al., 2016). The northward and westward migration of rollback of the Tajik lithosphere should have increased the subsidence rate in the Tajik basin as its substratum subsided. This may have contributed to the transgression (back-stepping) of the Tavildara and Karanak Fm deposits onto the previously eroded Pamir hinterland. The waning and ultimately vanishing of growth strata in the upper Tavildara Fm (~7 Ma) and deposition of the fine-grained floodplain strata of the Karanak Fm (~5–4 Ma) may reflect this lithospheric process in the Shurobod area. The change to fine-grained deposits correlates with a major decrease in shortening rates in the distal (northwestern) Tajik fold-thrust belt and its western and northern forelands, and the concentration of shortening in the proximal (eastern) Tajik basin (Abdulhameed et al., 2020). This effect of a rolling back lithosphere on the Tajik basin may be similar to the model proposed by Schlunegger and Kissling (2015) for the northern Alps. Since it is contested that the large-scale subsidence pattern of a basin and accumulation of kilometer-thick sedimentary fan successions can be explained through build-up of topographic loads alone (Pfiffner et al., 2002), they suggested that rollback of the subducting plate in a continent-continent collision regime is likely to account for a good part of the formation of accommodation space in the foreland basin. The evolution of the Tajik basin with its distinct stages of synorogenic deposition thus offers insights into the strongly coupled relationship of the development of the Pamir, plate processes at depth, and their effects on the sedimentary system at the surface. The ultimate verification of these correlations, however, awaits better dating of the synorogenic strata in the Tajik basin.

7. Conclusions

Following the final retreat of the Paratethys during the late Eocene, the eastern Tajik basin evolved from an epi-continental sag basin into an exclusively terrestrial foreland basin with a distal alluvial plain. The distal to proximal and coarse fan deposits of the Baljuvon Formation (~34–23 Ma) in the Shurobod area were contemporaneous with crustal thickening in the South and Central Pamir at ≥ 37 Ma, in particular with accelerated thickening at ~27–20 Ma. The main phase of proximal synorogenic sediment accumulation in the Tajik basin in the Khingou Formation ($\leq \sim 23$ –15 Ma) led to the development and coalescence of alluvial fans into an extended bajada in close proximity to the hinterland. This was likely triggered by the relocation of the deformation front from the Central Pamir to the North Pamir during the main phase of extensional collapse (foreland advance) of the Central Pamir (~23–12 Ma). The largest oversized clasts in the lower Khingou Formation are contemporaneous with peak erosion in the South and Central Pamir (~23–20 Ma). The onset of the basin reconfiguration from a foreland basin into a fold-thrust belt is indicated by the appearance of growth strata in the middle Khingou Formation of the Shurobod area. Prominent growth strata in the Tavildara Formation ($\leq \sim 15$ –5 Ma) signal the main phase of fold-thrust belt formation. Headward erosion and growth of transverse streams through drainage-divide migration and cannibalization of drainage basins led to the development of fluvial megafans. This coincided with the onset of the rollback of the Tajik lithosphere at ~12–11 Ma, which initiated the advance of the Pamir-plateau crust into the Afghan-Tajik depression. The absence of growth strata in the upper Tavildara Formation (~7 Ma) and the presence of fine-grained floodplain deposits in the Karanak Formation (~5–4 Ma) likely reflects a deepening of the eastern Tajik basin caused by northward and westward migration of the rollback of the Tajik-basin lithosphere. This was accompanied by a decrease in shortening rates in the Tajik basin and a back-stepping (transgression) of deposition onto the previously eroded western Pamir flank. To better constrain the development of the Tajik basin, and the information it provides about the development of the Pamir, it is imperative to establish a more precise timeframe for the synorogenic strata.

Acknowledgments

Additional data are given in the supporting information and can be downloaded from <https://doi.org/10.25532/OPARA-53>. Funded by the German Federal Ministry of Education and Research (support code 03G0809) as part of the CAME project bundle TIPTIMON. TIPTIMON field-team members were C. Auffermann, M. Berger, E. Kanaev, V. Minaev, and F. Sharopov. A Research Fellowship from the A. V. Humboldt Foundation funded A. Szulc's work at Freiberg. We thank the entire TIPTIMON group (GFZ Potsdam, Universität Jena, TU Bergakademie Freiberg, and UCSB) for discussion and support. We gratefully acknowledge the reviews by M. Jolivet and M. Brookfield. Open access funding enabled and organized by Projekt DEAL.

References

- Abdulhameed, S., Ratschbacher, L., Jonckheere, R., Gągała, Ł. R., Enkelmann, E., Kars, M., et al. (2020). Tajik Basin and southwestern Tian Shan, northwestern India-Asia collision zone: 2. Timing of basin inversion, Tian Shan mountain building, and relation to Pamir-Plateau advance and deep India-Asia Indentation. *Tectonics*, 39. <https://doi.org/10.1029/2019TC005873>
- Allen, M.-B., Windley, B.-F., Zhang, C., Zhao, Z.-Y., & Wang, G.-R. (1991). Basin evolution within and adjacent to the Tien Shan Range, NW China. *Journal of the Geological Society of London*, 148, 369–378.
- Babaev, A. (1988). Tectonic boundary between the Gissar-Alai and Tajik depression. *Bulleten Moskovskogo Obščestva Ispytatelej Prirody, Otd Geol.*, 63(3), 23–30. (in Russian)
- Bande, A., Sobel, E. R., Mikolaichuk, A., & Torres, A. V. (2015). Talas–Fergana Fault Cenozoic timing of deformation and its relation to Pamir indentation. In M.-F. Brunet, T. McCann, & E. R. Sobel (Eds.), *Geological evolution of Central Asian Basins and the Western Tien Shan Range*. *Geol. Soc., London, Spec. Publ.* (Vol. 427, pp. 295–311). London, UK: Geological Society of London. <https://doi.org/10.1144/SP427.1>
- Beaumont, C., Fullsack, P., & Hamilton, J. (1992). Erosional control of active compressional orogens. In K.-R. McClay (Ed.), *Thrust Tectonics* (pp. 1–18). London, UK: Chapman & Hall.
- Bosboom, R., Dupon-Nivet, G., Grothe, A., Brinkhuis, H., Villa, G., Mandic, O., et al. (2013). Linking Tarim Basin sea retreat (west China) and Asian aridification in the late Eocene. *Basin Research*, 26, 1–20.
- Bosboom, R., Dupon-Nivet, G., Houben, A.-J.-P., Brinkhuis, H., Villa, G., Mandic, O., et al. (2011). Late Eocene sea retreat from the Tarim Basin (west China) and concomitant Asia paleoenvironmental change. *Palaeogeography, Palaeoclimatology, Palaeoecology*, 299, 385–398.
- Bosboom, R., Mandic, O., Dupon-Nivet, G., Proust, J.-N., Ormukov, C., & Aminov, J. (2015). Late Eocene palaeogeography of the proto-Paratethys Sea in Central Asia (NW China, southern Kyrgyzstan and SW Tajikistan). *Geological Society, London, Special Publications*, 427, 565–588.
- Bosov, V.-D. (1961). *About the Late Tertiary deposits of the Eastern Tajik depression*. Tajik, USSR: Geological Institute, Academy of Sciences Press. (in Russian)
- Bosov, V.-D. (1972). *Tertiary continental deposits of Tajikistan*. Dushanbe, USSR: Donish. (in Russian)
- Bull, W.-B. (1977). The alluvial-fan environment. *Progress in Physical Geography*, 1(2), 222–270.
- Burtman, V.-S., & Molnar, P. (1993). Geological and geophysical evidence for deep subduction of continental crust beneath the Pamir. *Geological Society of America Special Papers*, 281, 1–76.
- Cain, S.-A., & Mountney, N.-P. (2009). Spatial and temporal evolution of a terminal fluvial fan system: The Permian organ rock formation, south-east Utah, USA. *Sedimentology*, 56, 1774–1800.
- Carrapa, B., DeCelles, P.-G., Wang, X., Clementz, M.-T., Mancin, N., Stoica, M., et al. (2015). Tectono-climatic implications of Eocene Paratethys regression in the Tajik basin of central Asia. *Earth and Planetary Science Letters*, 424, 168–178.
- Castelltort, S., & Simpson, G. (2006). River spacing and drainage network growth in widening mountain ranges. *Basin Research*, 18(3), 267–276.
- Chapman, J. B., Carrapa, B., Ballato, P., DeCelles, P. G., Worthington, J., Oimahmadov, I., et al. (2017). Intracontinental subduction beneath the Pamir Mountains: Constraints from thermokinematic modeling of shortening in the Tajik fold-and-thrust belt. *Geological Society of America Bulletin*, 129, 1450–1471.

- Chapman, J. B., Carrapa, B., DeCelles, P. G., Worthington, J., Mancin, N., Cobianchi, M., et al. (2019). The Tajik Basin: A composite record of sedimentary basin evolution in response to tectonics in the Pamir. *Basin Research*. <https://doi.org/10.1111/bre.12381>
- Chapman, J. B., Scoggin, S. H., Kapp, P., Carrapa, B., Ducea, M. N., Worthington, J., et al. (2018). Mesozoic to Cenozoic magmatic history of the Pamir. *Earth and Planetary Science Letters*, *482*, 181–192.
- Clevis, Q., de Boer, P., & Wachter, M. (2003). Numerical model of drainage basin evolution and three-dimensional alluvial fan stratigraphy. *Sedimentary Geology*, *163*, 85–110.
- Cohen, K.-M., Finney, S.-C., Gibbard, P.-L., & Fan, J.-X. (2013). The ICS International Chronostratigraphic Chart. *Episodes*, *36*(3), 199–204.
- Colomera, L., Moutney, N.-P., & McCaffrey, W.-D. (2013). A quantitative approach to fluvial facies models: Methods and example results. *Sedimentology*, *60*, 1526–1558.
- Das, B.-K., Al-Mikhlaifi, A.-S., & Kaur, P. (2006). Geochemistry of Mansar Lake sediments, Jammu, India: Implication for source-area weathering, provenance, and tectonic setting. *Journal of Asian Earth Sciences*, *26*, 649–668.
- Davidzon, R.-M., Kreydenkov, G.-P., & Salibaev, G.-H. (1982). *Stratigraphy of Palaeogene deposits of the Tadjik Depression and adjacent areas*. Dushanbe: Donish. (In Russian)
- DeCelles, P., Gehrels, G., Quade, J., Ohja, T., Kapp, P., & Upreti, B. (1998). Neogene foreland basin deposits, erosional unroofing, and the kinematic history of the Himalayan fold-and-thrust belt, western Nepal. *Geological Society of America Bulletin*, *110*(1), 2–21.
- DeCelles, P., & Giles, K. (1996). Foreland basin systems. *Basin Research*, *8*, 105–123.
- DeCelles, P., Kapp, P., Quade, J., & Gehrels, G. (2011). Oligocene-Miocene Kailas basin, southwestern Tibet: Record of post-collisional upper-plate extension in the Indus-Yarlung suture zone. *Geological Society of America Bulletin*, *123*(7/8), 1337–1362.
- Descourvieres, C., Douglas, G., Leyland, L., Hartog, N., & Prommer, H. (2011). Geochemical reconstruction of the provenance, weathering and deposition of detrital-dominated sediments in the Perth Basin: The Cretaceous Leederville Formation, south-west Australia. *Sedimentary Geology*, *236*, 62–76.
- Dickinson, W.-R. (1970). Interpreting detrital modes of graywacke and arkose. *Journal of Sedimentary Petrology*, *40*(2), 695–707.
- Dickinson, W. R., Beard, L. S., Brakenridge, G. R., Erjavec, J.-L., Ferguson, R. C., Inman, K. F., et al. (1983). Provenance of North American Phanerozoic sandstones in relation to tectonic setting. *Geological Society of America Bulletin*, *94*, 222–235.
- Dzhalilov, M. R., Alekseev, M. N., Andreev, Y. N., & Salibaev, G. K. (1982). Mesozoic and Cenozoic deposits of the northern part of the Afghano-Tajik basin. In *Stratigraphic correlation between sedimentary basins of the ESCAP region, United Nations mineral resources development series* (Vol. III, ESCAP atlas of stratigraphy III, 48, pp. 131–137). New York.
- Einsele, G. (1996). Event deposits: The role of sediment supply and relative sea-level changes—Overview. *Sedimentary Geology*, *104*(1–4), 11–37.
- Feng, R., & Kerrich, R. (1990). Geochemistry of fine-grained clastic sediments in the Archean Abitibi greenstone belt, Canada: Implications for provenance and tectonic setting. *Geochimica et Cosmochimica Acta*, *54*, 1061–1081.
- Folk, R. L. (1974). *Petrology of sedimentary rocks* (p. 159). Austin, Texas: Hemphill Publishing.
- Forsten, A., & Sharapov, S. (2000). Fossil equids (Mammalia, Equidae) from the Neogene and Pleistocene of Tadzhikistan. *Geodiversitas*, *22*(2), 293–314.
- Frostick, L. E., & Jones, S. J. (2002). Impact of periodicity on sediment flux in alluvial systems: Grain to basin scale. In S. J. Jones, & L. E. Frostick (Eds.), *Sediment flux to basins: Causes, controls and consequences*, Geological Society, London, Special Publications (Vol. 191, pp. 81–95). London, UK: Geological Society of London.
- Gagała, Ł., Ratschbacher, L., Ringenbach, J.-C., Kufner, S.-K., Schurr, B., Dedow, R., et al. (2020). Tajik basin and southwestern Tian Shan, northwestern India-Asia collision zone: 1. Structure, kinematics, and salt-tectonics in the Tajik fold-and-thrust belt of the western foreland of the Pamir. *Tectonics*, *39*. <https://doi.org/10.1029/2019TC005871>
- Gallet, S., Jahn, B., & Torii, M. (1996). Geochemical characterization of the Luochan loess paleosol sequence, China, and paleoclimatic implications. *Chemical Geology*, *133*, 67–88.
- Gazzi, P. (1966). Le arenarie de flysch sopracretaceo dell'Appennino modenese: correlazioni con il flysch di Monghidoro. *Mineralogica e Petrografica Acta*, *12*, 69–97.
- Gibling, M. R. (2006). Width and thickness of fluvial channel bodies and valley fills in the geological record: A literature compilation and classification. *Journal of Sedimentary Research*, *76*, 731–770.
- Gradstein, F., Ogg, J., Schmitz, M., Ogg, G. (2012). *The geologic time scale 2012*. 2-Volume Set. Elsevier Science Publishing Co., Amsterdam, Netherlands. 1176 p.
- GRI (1961-1965). *Geological maps of the Soviet Union 1:200,000, Alai-Gissar, Pamir and South Tajikistan Series*, Nedra, Moscow: Russ. Geol. Res. Inst. (in Russian)
- Gubin, I. Y. (1960). *Patterns of seismic activity in Tadzhikistan* (p. 450). Academy of Sciences: Moscow. (in Russian)
- Hacker, B. R., Ratschbacher, L., Rutte, D., Stearns, M. A., Malz, N., Stübner, K., et al. (2017). Building the Pamir-Tibet Plateau—Crustal stacking, extensional collapse, and lateral extrusion in the Pamir: 3. Thermobarometry and petrochronology of deep Asian crust. *Tectonics*, *36*, 1743–1766. <https://doi.org/10.1002/2017TC004488>
- Hamburger, M. W., Sarewitz, D. R., Pavlis, T. L., & Popandopulo, G. A. (1992). Structural and seismic evidence for intracontinental subduction in the Peter the First Range, Central Asia. *Geological Society of America Bulletin*, *104*, 397–408.
- Haq, B. U., Hardenbol, J., & Vail, P. R. (1987). Chronology of fluctuating sea level since the Triassic. *Science*, *235*, 1156–1167.
- Helmold, K. P. (1985). Provenance of feldspathic sandstones—The effect of diagenesis on provenance interpretations: A review. In G. G. Zuffa (Ed.), *Provenance of Arenites* (pp. 139–163). Dordrecht: D. Reidel Pub Co.
- Herron, M. M. (1988). Geochemical classification of terrigenous sands and shales from core log data. *Journal of Sedimentary Petrology*, *58*, 820–829.
- Horton, B. K., & DeCelles, P. G. (2001). Modern and ancient fluvial megafan in the foreland basin system of the central Andes, southern Bolivia: Implications for drainage network evolution in fold-thrust belts. *Basin Research*, *13*, 43–63.
- Hu, Z., & Gao, S. (2008). Upper crustal abundances of trace elements: A revision and update. *Chemical Geology*, *253*, 205–221.
- Ingersoll, R. V., Bullard, T. F., Ford, R. L., Grimm, J. P., & Pickle, J. D. (1984). The effect of grain size on detrital modes: A test of the Gazzi-Dickinson point-counting method (Holocene, sand, New Mexico, USA). *Journal of Sedimentary Petrology*, *54*, 103–116.
- Ingersoll, R. V., & Suczek, C. A. (1979). Petrology and provenance of Neogene sand from Nicobar and Bengal fans, DSDP sites 211 and 218. *Journal of Sedimentary Petrology*, *49*(4), 1217–1228.
- Jones, N. S., Holliday, D. W., & McKervey, J. A. (2011). Warwickshire Group (Pennsylvanian) red-beds of the Canonbie Coalfield, England-Scotland border, and their regional palaeogeographical implications. *Geological Magazine*, *148*(1), 50–77.

- Käßner, A., Ratschbacher, L., Jonckheere, R., Enkelmann, E., Khan, J., Sonntag, B.-L., et al. (2016). Cenozoic intracontinental deformation and exhumation at the northwestern tip of the India-Asia collision-southwestern Tian Shan, Tajikistan, and Kyrgyzstan. *Tectonics*, *35*, 2171–2194. <https://doi.org/10.1002/2015TC003897>
- Kaya, M. Y., Dupont-Nivet, G., Proust, J.-N., Roperch, P., Bougeois, L., Meijer, N., et al. (2019). Paleogene evolution and demise of the proto-Paratethys Sea in Central Asia (Tarim and Tajik basins): Role of intensified tectonic activity at ca. 41 Ma. *Basin Research*, *31*(3), 461–486.
- Klocke, M., Voigt, T., Kley, J., Pfeifer, S., Rocktäschel, T., Keil, S., & Gaupp, R. (2017). Cenozoic evolution of the Pamir and Tien Shan mountains reflected in syntectonic deposits of the Tajik Basin. In M.-F. Brunet, T. McCann, & E. R. Sobel (Eds.), *Geological evolution of Central Asian Basins and the Western Tien Shan Range*, Geological Society, London, Special Publications (Vol. 427, pp. 523–564). <https://doi.org/10.1144/SP427.7>
- Kondur, V. P., Saf'yan, L. M., & Marsal, A. M. (1974). *Principal results of stratigraphic drilling in unexposed areas of southwestern Tajikistan. In Issues of the petroleum potential of Tajikistan*, Trudy TO VNIGRI, 6, (Vol. 159, pp. 21–31). Dushanbe: Donish.
- Koons, P. O. (1995). Modeling the topographic evolution of collisional belts. *Annual Review of Earth and Planetary Sciences*, *23*, 375–408.
- Kreydenkov, G., & Raspopin, V. (1972). Palaeogene of the southern Kirgizia. In K. Pomazkov (Ed.), *Geologia SSSR* (Vol. 25, pp. 237–250). Moscow: Nedra. (in Russian)
- Kufner, S.-K., Schurr, B., Ratschbacher, L., Murodkulov, S., Abdulhameed, S., Ischuk, A., et al. (2018). Seismotectonics of the Tajik Basin and surrounding mountain ranges. *Tectonics*, *37*, 2404–2424. <https://doi.org/10.1029/2017TC004812>
- Kufner, S.-K., Schurr, B., Sippl, C., Yuan, X., Ratschbacher, L., Akbar, A.-M., et al. (2016). Deep India meets deep Asia: Lithospheric indentation, delamination and break-off under Pamir and Hindu Kush (Central Asia). *Earth and Planetary Science Letters*, *435*, 171–184.
- Leith, W. (1982). Rock assemblages in Central Asia and the evolution of the Southern Asian Margin. *Tectonics*, *1*, 303–318.
- Leith, W., & Alvarez, W. (1985). Structure of the Vakhsh fold-and-thrust belt, Tadjik SSR: Geologic mapping on a Landsat image base. *Geological Society of America Bulletin*, *96*, 875–885.
- Leith, W., Simpson, D.-W., & Alvarez, W. (1981). Structure and permeability: Geologic controls on induced seismicity at Nurek reservoir, Tajikistan, USSR. *Geology*, *9*, 440–444.
- Leonov, J. G. (1977). *Documents about the geology of the Afghan-Tadjik Depression Problem Commission 9, Working Group 3–3: The tectonic regime of molasse-forming periods*. Moscow: Academy of Sciences Press. (in Russian)
- McLennan, S. M. (1989). Rare earth elements in sedimentary rocks: Influence of provenance and sedimentary processes. In B.-R. Lipin, & G.-A. McKay (Eds.), *Geochemistry and mineralogy of rare earth elements, Reviews in Mineralogy* (Vol. 21, pp. 169–200). Chantilly, VA: Mineralogical Society of America.
- McLennan, S. M., Hemming, D. K., & Hanson, G. N. (1993). Geochemical approaches to sedimentation, provenance and tectonics. *Geological Society of America Special Papers*, *284*, 21–40.
- McPherson, J. G. (1979). Calcrete (caliche) palaeosols in fluvial redbeds of the Aztec Siltstone (Upper Devonian), southern Victoria Land, Antarctica. *Sedimentary Geology*, *22*, 267–285.
- Muhs, D. R., Bettis, E. A., Been, J., & McGeehin, J. P. (2001). Impact of climate and parent material on chemical weathering in loess-derived soils of the Mississippi River valley. *Soil Science Society of America Journal*, *65*(6), 1761–1777.
- Mukherjee, S. (2013). *The science of clays* (p. 335). Netherlands: Springer.
- Murali, A. V., Parthasarathy, R., Mahadevan, T. M., & Sankar Das, M. (1983). Trace elements characteristics, REE patterns and partition coefficients of zircons from different geological environments - a case study on Indian zircons. *Geochimica et Cosmochimica Acta*, *47*, 2047–2052.
- Najman, Y., Bickle, M. J., Garzanti, E., Pringle, M., Barfod, D., Brozovic, N., et al. (2009). Reconstructing the exhumation history of the Lesser Himalaya, NW India, from a multi-technique provenance study of the foreland basin Siwalik Group. *Tectonics*, *28*, TC5018. <https://doi.org/10.1029/2009TC002506>
- Nance, W. B., & Taylor, S. R. (1976). Rare earth element patterns and crustal evolution—I. Australian post-Archean sedimentary rocks. *Geochimica et Cosmochimica Acta*, *40*(12), 1539–1551.
- Nemec, W., & Steel, R. J. (1984). Alluvial and coastal conglomerates: Their significant features and some comments on gravelly mass-flow deposits. In E. H. Koster, & R. J. Steel (Eds.), *Sedimentology of Gravels and Conglomerates, Canadian Society of Petroleum Geologists Memoir* (pp. 1–31). Canadian Society of Petroleum Geologists.
- Nichols, G., & Fisher, J. (2007). Processes, facies and architecture of fluvial distributary system deposits. *Sedimentary Geology*, *195*, 75–90.
- Nikolaev, V. (2002). Afghan-Tajik depression: Architecture of sedimentary cover and evolution. *Russian Journal of Earth Sciences*, *4*(6), 399–421.
- Pfiffner, O.-A., Schlunegger, F., & Buitert, S. (2002). The Swiss Alps and their peripheral foreland basin: Stratigraphic response to deep crustal processes. *Tectonics*, *21*(2), 1009. <https://doi.org/10.1029/2000TC900039>
- Popov, S., Rögl, F., Rozanov, A. Y., Steininger, F. F., Shcherba, I. G., & Kovac, M. (2004). Lithological-paleogeographic maps of Paratethys—10 maps Late Eocene to Pliocene. *Courier Forschungsinstitut Senckenberg*, *250*, 1–46.
- Potter, P.-E. (1978). Petrology and chemistry of big river sands. *Journal of Geology*, *86*, 423–449.
- Pozzi, J. P., & Feinberg, H. (1991). Paleomagnetism in the Tajikistan: Continental shortening of European margin in the Pamirs during Indian Eurasian collision. *Earth and Planetary Science Letters*, *103*, 365–378.
- Replumaz, A., Negro, A. M., Guillot, S., & Villasenor, A. (2010). Multiple episodes of continental subduction during India/Asia convergence: Insight from seismic tomography and tectonic reconstruction. *Tectonophysics*, *483*, 125–134.
- Rey, P. F., Teyssier, C., & Whitney, D. L. (2010). Limit of channel flow in orogenic Plateaux. *Lithosphere*, *2*(5), 328–332. <https://doi.org/10.1130/L114.1>
- Rudnick, R. L., & Gao, S. (2003). Composition of the continental crust. In R. L. Rudnick, H.-D. Holland, & K.-K. Turekian (Eds.), *The Crust, Treatise on Geochemistry* (Vol. 3, pp. 1–64). Oxford: Elsevier-Perгамon.
- Rutte, D., Ratschbacher, L., Khan, J., Stübner, K., Hacker, B.-R., Stearns, M.-A., et al. (2017). Building the Pamir-Tibetan Plateau—Crustal stacking, extensional collapse, and lateral extrusion in the Central Pamir: 2. Timing and rates. *Tectonics*, *36*, 385–419. <https://doi.org/10.1002/2016TC004294>
- Rutte, D., Ratschbacher, L., Schneider, S., Stübner, K., Stearns, M.-A., Gulzar, M.-A., & Hacker, B.-R. (2017). Building the Pamir-Tibetan plateau—Crustal stacking, extensional collapse, and lateral extrusion in the Central Pamir: 1. Geometry and kinematics. *Tectonics*, *36*, 342–384. <https://doi.org/10.1002/2016TC004293>
- Sass, P., Ritter, O., Ratschbacher, L., Timpel, J., Matiukov, V. E., Rybin, A. K., & Batalev, V. Y. (2014). Resistivity structure underneath the Pamir and Southern Tian Shan. *Geophysical Journal International*, *198*(1), 564–579. <https://doi.org/10.1093/gji/ggu146>

- Schlunegger, F., & Kissling, E. (2015). Slab rollback orogeny in the Alps and evolution of the Swiss Molasse basin. *Nature Communications*, 6, 8605. <https://doi.org/10.1038/ncomms9605>
- Schneider, F. M., Yuan, X., Schurr, B., Mechie, J., Sippl, C., Kufner, S.-K., et al. (2019). The crust in the Pamir: Insights from receiver functions. *Journal of Geophysical Research: Solid Earth*, 124, 9313–9331. <https://doi.org/10.1029/2019JB017765>
- Schurr, B., Ratschbacher, L., Sippl, C., Gloaguen, R., Yuan, X., & Mechie, J. (2014). Seismotectonics of the Pamir. *Tectonics*, 33, 1501–1518. <https://doi.org/10.1002/2014TC003576>
- Schwab, G., Katzung, G., Ludwig, A.-O., & Lützner, H. (1980). Neogene molasse-sedimentation in der Tadschikischen depression (tadschikische SSR). *Zeitschrift der Angewandten Geologie*, 26, 225–238. (in German)
- Shukla, U. K., Singh, I. B., Sharma, M., & Sharma, S. (2001). A model of alluvial megafan sedimentation: Ganga Megafan. *Sedimentary Geology*, 144, 234–262.
- Simakov, S. (1952). About the stratigraphy of the Palaeogene of the Ferghana Basin and Tadjik depression. *Doklady Akademii Nauk SSSR*, 31, 147–150. (in Russian)
- Sippl, C., Schurr, B., Tynpel, J., Angiboust, S., Mechie, J., Yuan, X., et al. (2013). Deep burial of Asian continental crust beneath the Pamir imaged with local earthquake tomography. *Earth and Planetary Science Letters*, 384, 165–177. <https://doi.org/10.1016/j.epsl.2016.12.043>
- Sippl, C., Schurr, B., Yuan, X., Mechie, J., Schneider, F. M., Gadoev, M., et al. (2013). Geometry of the Pamir-Hindu Kush intermediate-depth earthquake zone from local seismic data. *Journal of Geophysical Research - Solid Earth*, 118, 1438–1457. <https://doi.org/10.1002/jgrb.50128>
- Smit, M. A., Ratschbacher, L., Kooijman, E., & Stearns, M. A. (2014). Early evolution of the Pamir deep crust from Lu-Hf and U-Pb geochronology and garnet-thermometry. *Geology*, 42(12), 1047–1050.
- Stearns, M. A., Hacker, B. R., Ratschbacher, L., Lee, J., Cottle, J. M., & Kylander-Clark, A. (2013). Synchronous Oligocene-Miocene metamorphism of the Pamir and the north Himalaya driven by plate-scale dynamics. *Geology*, 41(10), 1071–1074.
- Stearns, M. A., Hacker, B. R., Ratschbacher, L., Rutte, D., & Kylander-Clark, A. R. C. (2015). Titanite petrochronology of the Pamir gneiss domes: Implications for middle to deep crust exhumation and titanite closure to Pb and Zr diffusion. *Tectonics*, 34, 784–802. <https://doi.org/10.1002/2014TC003774>
- Stübner, K., Ratschbacher, L., Rutte, D., Stanek, K., Minaev, V., Wiesinger, M., & Gloaguen, R. (2013). The giant Shakh-dara migmatitic gneiss dome, Pamir, India-Asia collision zone: 1. Geometry and kinematics. *Tectonics*, 32, 948–979. <https://doi.org/10.1002/tect.20057>
- Stübner, K., Ratschbacher, L., Weise, C., Chow, J., Hofmann, J., Khan, J., et al. (2013). The giant Shakh-dara migmatitic gneiss dome, Pamir, India-Asia collision zone: 2. Timing of dome formation. *Tectonics*, 32, 1–28. <https://doi.org/10.1002/tect.20059>
- Sun, J., & Jiang, M. (2013). Eocene seawater retreat from the southwest Tarim Basin and implications for early Cenozoic tectonic evolution in the Pamir Plateau. *Tectonophysics*, 588, 27–38.
- Taylor, S. R., & McLennan, S. M. (1985). *The continental crust: Its composition and evolution* (p. 312). Oxford: Blackwell Scientific Publications.
- Thomas, J. C., Chauvin, A., Gapais, D., Bazhenov, M. L., Perroud, H., Cobbold, P., & Burtman, V.-S. (1994). Paleomagnetic evidence for Cenozoic block rotations in the Tadjik depression (central Asia). *Journal of Geophysical Research*, 99, 15,141–15,160.
- Trifonov, V. G. (1978). Late Quaternary tectonic movements of western and central Asia. *Geological Society of America Bulletin*, 89(7), 1059–1072.
- Vail, P. R., & Mitchum, R. Jr. (1979). Global cycles of relative changes of sea level from seismic stratigraphy: Resources, comparative structure, and eustatic changes in sea level. In J.-S. Watkins (Ed.), *Geological and geophysical investigations of continental margins, AAPG Memoir 29, American Association of Petroleum Geologists* (pp. 469–472). Tulsa, OK.
- Vjalov, O. (1940). *Stratigraphy of the Palaeogene of the Tadjik depression* (Vol. 129, pp. 3–55). Leningrad: Trudy Neftjanogo Instituta.
- Vlasov, N. G., Dyakov, Y. A., & Cherev, E. S. (1991). *Geological map of the Tajik SSR and adjacent territories, 1:500,000*. Leningrad, Saint Petersburg: Vsesojuznoi Geol. Inst.
- Wang, W., Kirby, E., Peizhen, Z., Dewen, Z., Guangliang, Z., Huiping, Z., et al. (2013). Tertiary basin evolution along the northeastern margin of the Tibetan Plateau: Evidence for basin formation during Oligocene transtension. *Geological Society of America Bulletin*, 125(3/4), 377–400.
- Wellman, H.-W. (1966). Active wrench fault of Iran, Afghanistan and Pakistan. *Geologische Rundschau*, 55(3), 716–735.
- Worthington, J. R., Ratschbacher, L., Stübner, K., Khan, J., Malz, N., Schneider, S., et al. (2020). The Alichur dome, South Pamir, western India-Asia collisional zone: Detailing the Neogene Shakh-dara-Alichur syn-collisional gneiss-dome complex and connection to lithospheric processes. *Tectonics*, 39. <https://doi.org/10.1029/2019TC005735>
- Xiao, G., Guo, Z., Dupon-Nivet, G., Lu, H., Wu, N., Ge, J., et al. (2012). Evidence for northeastern Tibetan Plateau uplift between 25 and 20 Ma in the sedimentary archive of the Xining Basin, Northwestern China. *Earth and Planetary Science Letters*, 317–318, 185–195.
- Zheng, H., Huang, X., & Butcher, K. (2006). Lithostratigraphy, petrography and facies analysis of the late Cenozoic sediments in the foreland basin of the West Kunlun. *Palaeogeography, Palaeoclimatology, Palaeoecology*, 241, 61–78.